12-2019

Understanding and Controlling Lithium Microstructure during Electroplating for Energy Applications

Yang Tian
University of Arkansas, Fayetteville

Understanding and Controlling Lithium Microstructure during Electroplating for Energy Applications

A thesis submitted in partial fulfillment
of the requirements for the degree of
Master of Science in Chemistry

by

Yang Tian
Beijing Institute of Technology
Bachelor of Engineering in Environmental Engineering, 2017

December 2019
University of Arkansas

This thesis is approved for recommendation to the Graduate Council.

Jie Xiao, Ph.D
Thesis Director

Ryan Tian, Ph.D
Committee Member

Robert Coridan, Ph.D
Committee Member

Jingyi Chen, Ph.D
Committee Member

ABSTRACT

Lithium-ion batteries are reaching the specific theoretical capacity limit, while lithium metal batteries are regarded as the ideal energy storage system for the next generation "beyond lithium-ion" battery systems. The lithium metal anode is considered as the "Holy grail" of anodes due to its relatively low electrochemical potential (-3.04 V vs SHE) and high theoretical capacity (3860 mAh g^{-1}). However, the application of lithium metal anodes is hindered because of significant reaction between metallic lithium and electrolytes, as well as uneven electro-plating, which leads to dendrite formation, causing safety problems.

The kinetic parameters of Li ions such as diffusion coefficient are strongly related to dendrite growth. In this thesis, micro-electrodes are employed to determine the diffusion coefficients in various electrolytes. Compared with SEM images of lithium metal microstructures obtained by electro-deposition, the lower diffusion coefficient can promote lithium dendrite growth at a similar exchange current density, which is indicated by Sand's equation. The low electro-chemical potential of lithium metal leads to reactions between the metallic lithium and the conventional electrolytes. However, the benzene possesses a lower electro-chemical potential (-3.42 V vs SHE). Therefore, benzene is applied as a co-solvent to adjust ionic solvation structures of the electrolytes for lithium anode protection.

In chapter 1, the background of lithium metal anodes is introduced. In chapter 2, the micro-electrodes are employed to determine the kinetic parameters of the electrolytes. Then the relations among these parameters and electro-plating morphologies are explored. In chapter 3, benzene is applied as a co-solvent in the electrolyte. The improved performance of the lithium

metal anode protection is shown in this chapter. Chapter 4 further investigates the benzene-based electrolytes as applied in lithium metal full-cell batteries, such as lithium-sulfur batteries and NCM-lithium metal batteries, and the performance is noted.

ACKNOWLEDGEMENTS

It is a great honor for me to express my honest and sincerest appreciation to my thesis advisor, Dr. Jie Xiao. I appreciate the helpful advice and suggestions in whatever research field and daily life. I feel very grateful to join her group and have precious opportunities to develop next-generation batteries, which is very helpful for my future research.

At the same time, I want to thank the rest of my committee members, Dr. Ryan Tian, Dr. Robert Coridan, and Dr. Jingyi Chen, for their great support, encouragement and advice about my research and self-improvement.

Besides my thesis committee, I'd like to thank my lab-mates, Dr. Bingbin Wu, Mrs. Dinyin Liu, Mr. Josh Lochala, and Mr. Witness Martin. They helped me a lot in my lab, and I learned much from them.

Last but not least, I really appreciate my parents. Thanks for their great support!

TABLE OF CONTENTS

LIST OF FIGURES

2 UNDERSTANDING THE LITHIUM DENDRITE GROWTH

1 INTRODUCTION

Battery energy storage systems have achieved great success in portable electronics, medical devices, and electric vehicles. [1] In particular, Li-ion batteries have been thoroughly explored and applied in industry and everyday consumer devices as rechargeable batteries due to their long lifespan, high safety, and relatively high capacity. However, Li-ion batteries are reaching their specific theoretical capacity limit while the markets demand for higher capacity continuously increases. [2] Metallic lithium is considered the ideal anode material for rechargeable batteries which possesses the advantages of lightweight (0.53 g cm^{-3}), high theoretical capacity (3860 mAh g^{-1}), and a relatively low electrochemical potential (-3.04 V vs. SHE). [2] Primary lithium metal batteries have mainly been around since the 1970s. [3] Nonetheless, rechargeable lithium metal anodes are severely impeded from practical applications due to the reaction between metallic lithium and the electrolytes, as well as uneven deposition which leads to massive dendrite growth causing safety problems and battery failures. These issues have been conducted to explore the mechanisms of lithium plating/stripping in an attempt to mitigate dendrite formation along with a relative infinite volume change deposition. [4]

In this chapter, the history of lithium metal anodes, mechanisms, as well as protection methods, will be discussed.

1.1 The development of lithium metal anode

In the 1950s, lithium metal was found to be stable in some of the nonaqueous solvents by forming a protection layer. [5] Following this discovery, lithium salts have been developed to

create Li^+ based electrolytes which are compatible with a lithium metal anode electrode. Until the 1970s, commercial lithium metal batteries were applied on a large scale in devices such as digital watches, implantable medical devices, and other portable devices. However, these batteries were of the primary batteries type, which can only be used once. This is disadvantageous because it increases the cost of use and poses a burden on the environment. Later, Dey with his company, Moli, commercialized the first generation of rechargeable lithium metal batteries where they used MoS_2 and other lattice materials as cathodes in the 1980s. [4] However, these batteries were commercially unsuccessful. The non-uniform deposition of lithium at the anode during the charging process caused a short circuit of the battery, resulting in significant safety problems.

It is considerably challenging to apply lithium metal anodes in rechargeable batteries due to the active reaction properties and uneven deposition of lithium metal. In 1991, Sony firstly successfully commercialized Li-ion batteries using graphite as the anode and $LiCoO_2$ as the cathode which is described as the “rocking chair battery” because lithium is stored as in state of lithium-ion rather than as a lithium metal anode. [1] Since then, lithium-ion batteries have been a hot topic of research for almost 30 years.

However, lithium-ion batteries are reaching their theoretical capacity limit. [5, 6] Market demand requires the production of batteries with a higher energy density. Potential candidates for this are batteries such as lithium-sulfur, lithium-air, and other lithium metal-based batteries. The most common challenge among these types of batteries is how to stabilize the lithium metal anode to

achieve even deposition without dendrite growth in the electrolytes.

1.2 The applications and challenges of lithium metal anodes

The lithium metal anode is an ideal replacement for the intercalation anodes, which is used in lithium-ion batteries as discussed above. Lithium metal is widely applied in many different types of batteries systems such as lithium-sulfur batteries and lithium-air batteries [7]. However, lithium metal as the anode is still facing with many considerable challenges such as low Coulombic efficiency, limited cycle number, and fatal dendrite growth, but it has various issues in different lithium metal batteries. For example, the lithium metal anode performs better when intercalation cathodes are used as opposed to cathodes, and sealed battery systems show more stable results of lithium metal anodes compared to open battery systems. [8-11] Therefore, it is worthwhile to investigate the challenges in distinct battery systems.

Lithium intercalation cathode batteries which are applied in conjunction with lithium metal as the anode have been intensely studied in recent years. One of the distinct advantages is that almost all the electrolytes used in lithium-ion batteries can be adopted in this battery system. However, the issues here are still severe. On the one hand, the phenomenon of lithium dendrite growth is significant. For example, Exxon developed Li||TiS batteries in the 1970s which caused severe safety problems. [1] On the other hand, lithium metal easily forms a solid electrolyte interface (SEI), and the continuous consumption of the electrolytes, which ultimately results in battery failure. Researchers are actively working to develop new electrolytes which are compatible with lithium metal anode and can form a durable and beneficial SEI layer on the

surface of the lithium. [3, 4, 8, 12-14]

Another application of lithium metal anode is in lithium-sulfur batteries which have been thoroughly studied in the last decade due to their high theoretical energy density (2567 Wh kg^{-1}) [6, 7, 15-18]. For this system, most researchers focus on finding solutions to issues related to the cathode rather than the lithium metal anode and its replacement. Only 3% of the articles published in battery research fields in the recent ten years targeted the concerns surrounding the lithium metal anodes. [1] As a result of the presence of polysulfides, there is a passivated layer that can be formed at the surface of lithium metal electrodes. Although this layer can protect the lithium dendrite growth, the electrolyte components progressively corrode the electrodes and results in the consumption of electrolytes. Ultimately, it can lead to the failure of the batteries due to extremely high impedance.

1.3 Lithium dendrite prevention and high Coulombic efficiency of lithium plating/stripping by SEI construction

As a result of the relatively lower electrochemical potential of metallic lithium, most the solvents cannot avoid reacting with the lithium metal anode in a battery. Even though these solvents are compatible with the lithium metal, they can be reduced at the low electrochemical potential of the lithium metal, forming a robust SEI layer at the surface of the anode which prevents further reaction between the lithium and the solvent. This SEI layer was first found by Dey in 1970, and it was found to be roughly 20 to 50 nm in thickness. [3, 4, 11, 19-21] In the 1970s, Goodenough et al., explained the formation mechanism of the SEI, which has become widely accepted. [1]

SEI indeed has a significant effect on the process of lithium nucleation and dendrite growth.

The protection of lithium metal anode has been investigated. One of the most successful methods to prevent lithium dendrite growth is the addition of electrolyte additives such as FEC (fluoroethylene carbonate) and VC (vinylene carbonate) co-solvents, and $LiNO_3$ salt to the primary solvent which is typically dioxolane (DOL) and 1,2 dimethoxyethane (DME). [3, 11, 12, 14, 19, 21-23] These additives contribute to the formation of a durable SEI at the anode surface during the charging/discharging processes because they form SEI component molecules such as LiF and LiN in the SEI which is considered beneficial for the preservation of the lithium metal surface.

Considering these known beneficial components of SEI, researchers have attempted to pretreat the surface of the lithium metal by synthesizing artificial SEI on the metal surface in a more controllable manner to prevent the undesired side reaction resulting from the addition of electrolytes additives. These pretreatments are classified as electrochemical pretreatment, chemical pretreatment, and physical pretreatment. Nevertheless, each method offers various handicaps. For instance, electrochemical pretreatment is an ex-situ method to construct reliable SEI. Chemical approaches such as chemical vapor deposition (CVD) and atomic layer deposition (ALD) although impressive, are still unclear on whether a single component SEI is better than a combined ingredient SEI. [24, 25] For physical treatment such as polymer membrane coated on the anode, the thickness and conductivity are significant for practical application.

In summary, the protection of the lithium metal anode has been relatively improved in terms of

Coulombic efficiency and lifespan in the last decade by the construction of durable SEI. Nonetheless, more insights about SEI components and the kinetics of electrode processes at the interface still need to be considered.

1.4 The mechanism of lithium metal anode dendritic formation in solutions

Even though the protection of lithium metal anode by building tenacious SEI has been made impressive progress in the aspect of Coulombic efficiency or service time, it is still challenging to apply these approaches in practical punch cells or large scale to meet the requirement of the industry. It is a temporary treatment which is not an intrinsic way to inhibit lithium dendrite growth. In addition to this, SEI is not the only aspect that dominates uneven lithium deposition. Lithium dendrites are decided by the diffusion process in electrolytes as well.

Henry Sand put forward the view that the concentration of Cu^{2+} becomes 0 at the surface of the electrode during copper deposition, which leads to hydrogen evolution. [1, 3, 4, 26, 27] This concept broadly accepted and extended to indicate the time when the lithium dendrites start growing, which is called “Sand’s time”. If lithium ions are consuming more rapidly than they are diffusing to the surface of lithium metal anode, then the lithium ions will be depleted at the surface of electrolde. If deposition continues towards the anode, lithium dendrites appear to grow. This process yields the equation,

$$\tau = \pi D\left(\frac{eC_0}{2Jt_a}\right)^2 \qquad (1)$$

Where τ is sand’s time, D, C_0, J, t_a is diffusion coefficient, bulk concentration, current density, transfer number of anions, respectively.

In this paper, the tools are employed to measure the kinetic parameters explaining the uneven deposition related to the diffusion process. Moreover, benzene is considered as a promising co-solvent for the first time, and the results of the electrochemical test have shown outstanding performances of benzene-based electrolytes in both lithium-sulfur batteries and NCM lithium metal batteries.

2 UNDERSTANDING THE LITHIUM DENDRITE GROWTH

Rechargeable lithium metal batteries have been considered one of the most promising energy storage system for the next-generation battery technologies due to lithium metal's (Li) light density (0.534 g cm^{-3}) and concentrated energy (3680 mAh g^{-1}). [4] However, Li is reactive in almost all liquid electrolytes producing a passivating solid electrolyte interphase (SEI) on the Li surface. [3] Although the presence of the SEI terminates the further side reactions between the Li and the electrolyte due to its electronic immobility nature, it interferes with the homogeneous distribution of the electrical field within the anode. The result is the uneven growth of Li. Besides, during cycling the SEI layers breaks down after Li is stripped and new SEI forms during Li deposition. [1] Continuous consumption of electrolyte is accompanied by the growth of the SEI and dead Li. Sometimes, the dendritic Li may penetrate through the separator raising the safety concerns. All these issues plague the large-scale deployment of rechargeable lithium metal batteries. [28-34]

2.1 Introduction of lithium dendrite formation by diffusion control

For dealing with the problems of rechargeable lithium metal anodes, the underlying causes for the uneven growth of Li metal need to be considered. Even without SEI layers, the electrochemical deposition of other metal such as Na or Zn is never smooth [1] which is intrinsically related to the mass transport of metal ions. [29] In the solution, the diffusion rate of lithium ions to the anode surface plays a vital role in forming the Li dendrites, which is very

similar to the electroplating process.[35] Fast transport of the plated ions (Li^+) to the slowly (low current density) plated electrode (Li) leads to a smooth and shiny metal layer during electroplating, while slow transport of the plated ions to the rapidly plated electrode (high current density) forms fibrous dendrites. This explains why the chances of forming dendritic Li is increased at high rates. It also partially explains why concentrated electrolyte, i.e. reduced Li^+ concentration gradient in the solution, helps to smooth out the Li dendrite. [36] In addition to the ion transportation in the liquid electrolyte, the reaction rate of the electrochemical reactions also needs to be considered and compared to the rate of the "supplying" ions from the electrolyte to the electrode surface.

In this chapter, we integrate different electrochemical measurement approaches to quantify the kinetic properties of Li^+ diffusion and deposition in various electrolytes in an attempt to develop an electrochemical tool to rapidly screen out the promising electrolyte recipes that may smooth out lithium dendrites. Microelectrodes are used in the electrochemical measurements to exclude the interference from convection and for high-speed signal responses, which will significantly accelerate the exploration process of new electrolytes for improving the reversibility of lithium metal anodes. [37, 38]

2.2 Electrochemical tools for characterization

Henry J. S. Sand found the relationship between an instance of hydrogen evolution (Sand's time) and the current density when he measured the diffusion coefficient of copper sulphate in 1901. [39] Then, the equation was concluded as,

$$\tau = \pi D\left(\frac{eC_0}{2Jt_a}\right)^2 \qquad (1)$$

Where τ is Sand's time (s), D is diffusion coefficient of metal ions ($cm^2\ s^{-1}$), e is electronic charge (C), C_0 is ion concentration in bulk electrolyte (mol cm^{-3}), J is current (A cm^{-2}),and t_a is the transference number of anions which is equal to (1-t_+). When plating Li on the anode at a constant current density, there must be a moment when the concentration of Li^+ at the electrode surface becomes zero. This moment is called sand's time. At specific lithium plating current density, Sand's time is decided by the diffusion coefficient of lithium ions.

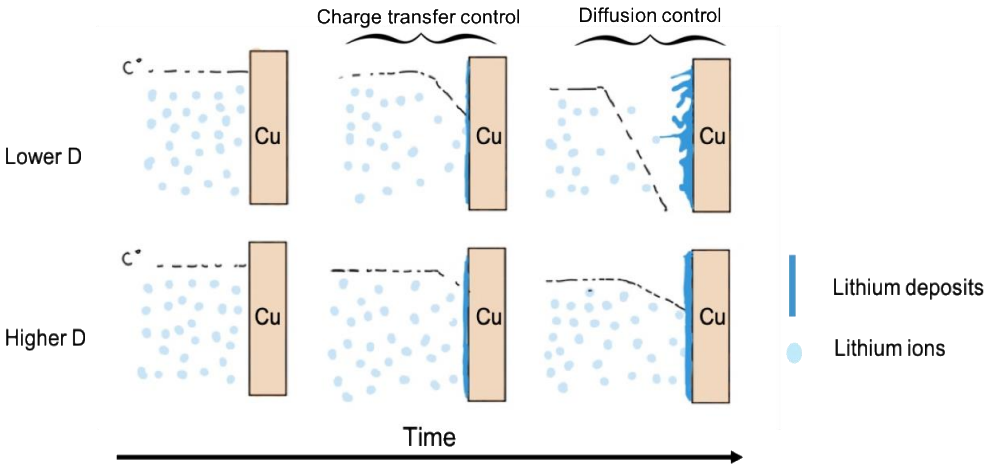

Figure 2.1 Schematic illustration of lithium deposition influenced by diffusion and charge transfer.

Stokes-Einstein equation describes the factors which can influence the diffusion coefficient.

$$D = \frac{k_B T}{6\pi\eta r} \qquad (2)$$

Where, k_B is Boltzmann constant, T is temperature, η is the viscosity, and r is ionic radii. One of the limitations for this equation is that it is mainly suitable for the experiment concerning the

temperature where the system diffusion coefficient generally decreases with increasing viscosity. Herein, a relationship between the diffusion coefficient and lithium morphologies is explored using micro-electrodes and various electrolytes. Furthermore, the study of the temperature and viscosity influence on the diffusion coefficients and lithium dendrite growth is analyzed.

2.2.1 Procedure of making micro-electrode

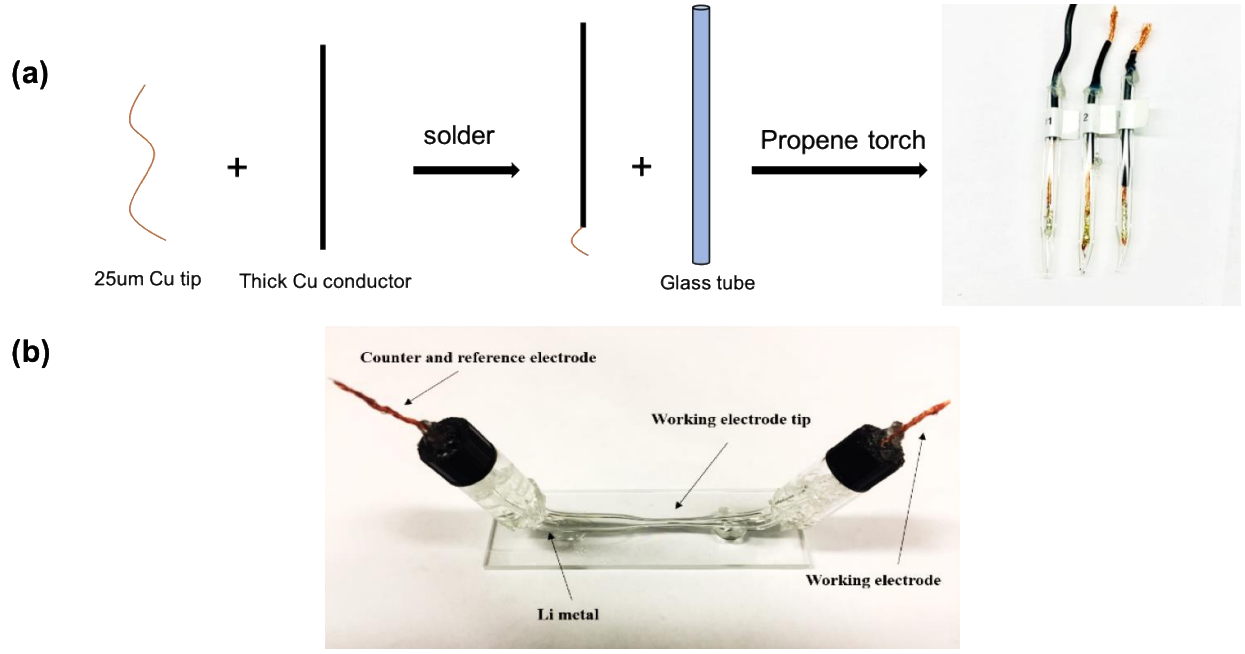

Figure 2.2 (a) Brief procedure of making 25 um diameter micro-electrode, and **(b)** homemade reactor for 125 um diameter micro-electrode to obtain SEI images.

Macro-electrodes are widely used in Li deposition studies such as coin cells, pouch cells, and some electrolytic cells. These macro-electrodes are easily influenced by convection, which causes a nonuniform current distribution and disturbs the diffusion layer due to the broad area of the electrodes. The micro-electrodes are used to measure the diffusion coefficient and to observe the morphologies of lithium deposits at the surface.

Two types of micro-electrode, the diameters of 25 um and 125 um were used. The 125 um

diameter Ni electrodes are purchased form Goodfellow coating with polyimide (PI) which is stable with electrolytes without further treatment.

The 25 um diameter micro-electrodes were homemade, and the brief procedure is shown in **Fig. 2.2.** The 25 um Cu wires were cut into 2 cm each, thick Cu conductors were cut into 7 cm each, and glass tubes were cut into 15 cm each. Then these materials were washed in DI water and ethanol three times by sonicating, respectively and dried at 60℃ in an oven overnight. Solder was used to connect 25 um Cu tip with the conductor. Then it was inserted into the glass tube. The tip was sealed under high temperature by propane torch. After the glass cooling down at the room temperature, the tip was polished by sandpapers of 400, 600, 1000, and 2000, coarseness grades respectively until the Cu tip was exposed. Then using Al_2O_3 nanoparticles, the micro-electrode tip was polished and cleaned by using DI water and ethanol three times respectively.

2.2.2 The principles of electro-chemical measurements

Bard et al. demonstrated the method to obtain the diffusion coefficient of $Fe(CN)^{4-}_6$ in KCl and borohydride in NaOH by applying chronoamperometry on a micro-electrode. [40] Here, the diffusion coefficient of lithium ions is determined by using the same way. The current at the micro-disk is

$$i_d\,(t) = nFC^{\circ}a^2\sqrt{\frac{\pi D}{t}} + 4nFDC^{\circ}a \qquad (3)$$

Where n, F, and c^* is the number of electrons involved in the electrode reaction, Faraday constant, and bulk concentration, respectively. Here, a is the radius of micro-disk.

The normalized **Eq. 3** with steady-state current is simplified to

$$\frac{i_d\,(t)}{i_{d,ss}} = \frac{\sqrt{\pi}}{4} a(Dt)^{-\frac{1}{2}} + 1 \qquad (4)$$

According to **Eq. 4**, $i_d(t)/i_{d,ss}$ has a linear relationship with $t^{-1/2}$ and n does not affect the calculation of the diffusion coefficient. A plot $i_d(t)/i_{d,ss}$ vs. $t^{-1/2}$ is a straight line which has the intercept of one and the slop S as shown in **Fig. 2.3**.

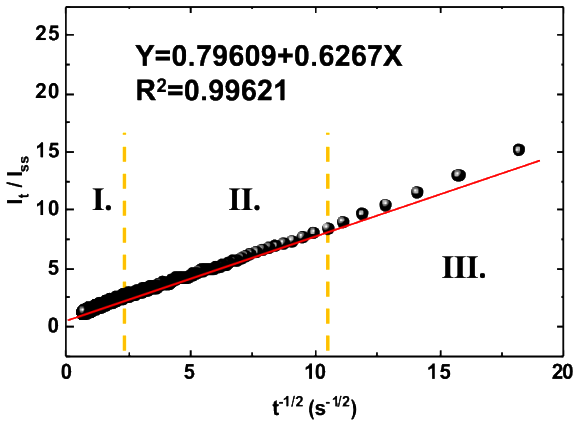

Figure 2.3 Chronoamperometry of lithium-ion deposition at 25 um micro-electrode in 1 M $LiClO_4$-PC, 23℃, potential step from 1 V to -0.015 V vs. Li^+/Li.

Thus, D is determined by

$$D = \frac{\pi a^2}{16S^2} \qquad (5)$$

The application of the above equations has to be without the effect of convection. The micro-disk radius is 12.5 um, which is small enough to prevent the influence of convection even after long times. However, the most significant difference here is that after lithium ions receive the electrons, lithium deposits on the surface of the electrode, which can increase the specific area of

the micro-electrode and influence the diffusion layer. Due to this reason, the data points in the region I in **Fig 2.3** were rejected. Compared with a long-time deposit, short time domain changes the surface area minimally. However, the current at micro-electrode can be affected by the charge of double layer and reactants adsorbed on the surface of micro-disk rather than the current response at the more extended time. [19] For this reason, data points in region III are also rejected.

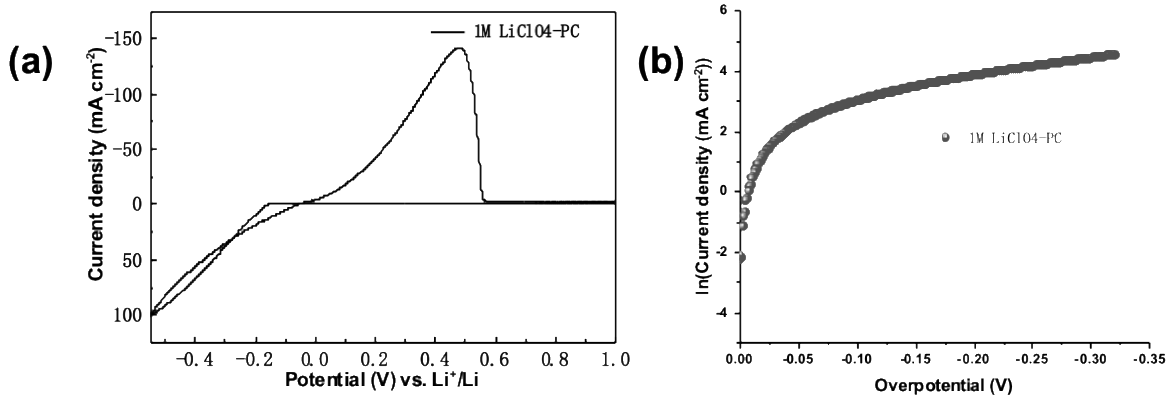

Figure 2.4 (a) Cyclic voltammetry results for the 125um Ni micro-electrode. Scan rate is 100 mV s^{-1} from 1 V to -0.35 V at 23℃. **(b)** Tafel plot.

Cyclic voltammetry results for a 125 um Ni micro-electrode are showed in **Fig 2.4 (a)**. The potential is initially set at 1 V vs. metallic lithium counter electrode. Then the potential was scanned from 1 V to -0.35 V. [41] The Bulter-Volmer equation is

$$j = j_0 \left(e^{(1-\beta) f \eta_s} - e^{-\beta f \eta_s} \right) \qquad (6)$$

where η_s is the overpotential, j_0 is the exchanged current density and β is the transfer coefficient. The Tafel equation can be written as,

$$\ln j = (1-\beta)\, f\eta_s \; + \ln j_0 \qquad (7)$$

Tafel plotted shown in **Fig. 2.4 (b)** are used to obtain the exchanged current density and transfer coefficient according to **Eq. 7** based on the first scan of the CV for the anodic current range.

2.3 Results and discussion

In this part, the effects of diffusion coefficients and the factors which influence diffusion coefficients will be discussed. The experiments are conducted using the micro-electrodes. The kinetic parameters, such as exchange current density and diffusion coefficients are determined. The morphology SEM images of lithium plating on the micro-electrodes which are related to the diffusion coefficients are collected for the first time.

2.3.1 Diffusion effects to lithium deposition morphologies

Linear sweep voltammetry was applied on the 125 um diameter Ni microelectrode. The scan rate is 130 mV s^{-1} from 1 V to -1.5 V, as shown in **Fig 2.5**. The morphologies of lithium deposits were obtained by SEM at different potentials. In the region I, the current density increases with potential growth. The morphologies of lithium metal in this region is relatively smooth without sharp dendrite growth. When the potential reaches the diffusion-controlled stage, the current density was growing slowly, but there is still no sharp dendrite growth. Once it arrived at the diffusion-controlled area in **Fig. 2.5 (a)** region II., the concentration of lithium-ion became 0, and the current density is constant, then the dendrites growing. The constant current density can only be kept for a while; then, it continues increasing. This is due to the surface area changing with

the deposition of lithium, as shown in **Fig. 2.5 (e) & (f)**. The diffusion layer is unstable at this point.

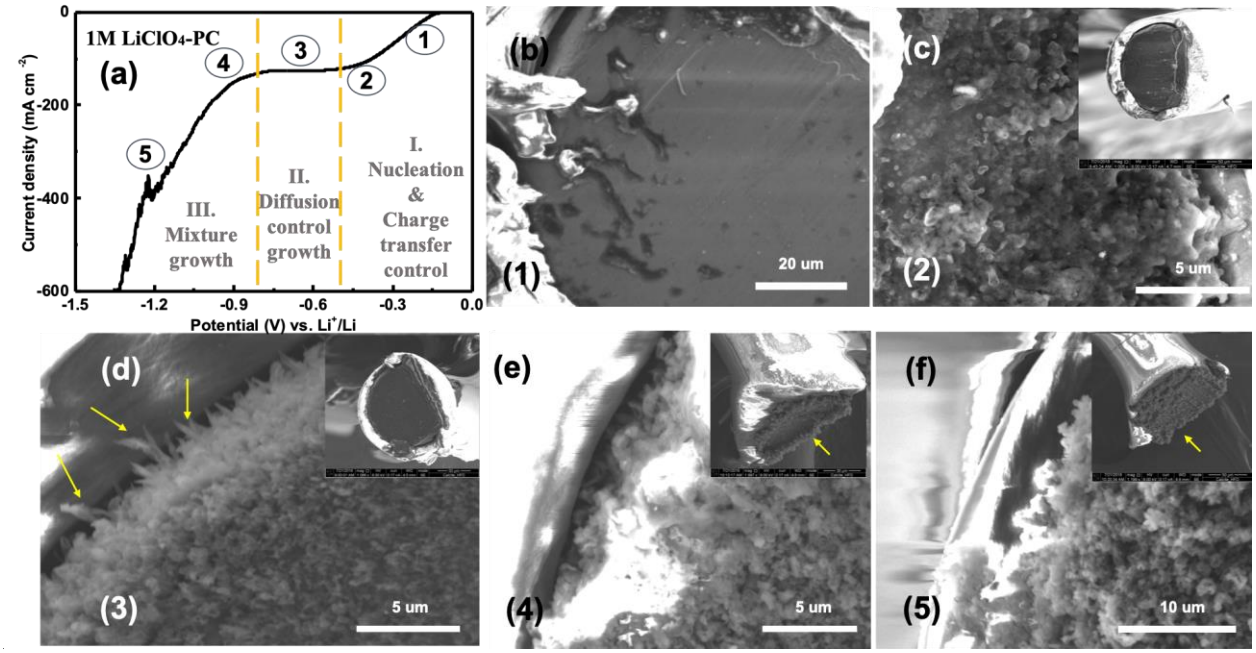

Figure 2.5 (a) LSV curve obtained by 125um micro-electrode. **(b)-(f)** SEM images of lithium-ion deposition at different potential on 100um micro-electrode in 1M $LiClO_4$-PC, potential step from 1 V to -1.5 V vs. Li^+/Li at 23℃ and scan rate is 130 mV s^{-1}.

The same method was used to study different types of electrolytes. PC-based electrolytes are shown in **Fig. 2.6 (a-d)** are 1M $LiPF_6$, LiTFSI, LiFSI, and $LiClO_4$ in PC, respectively. The scan rate is 20 mV s^{-1} from 1V to -0.35 V. The morphologies of lithium deposits are changing with the diffusion coefficient. This is because, in this condition, some electrolytes such as $LiClO_4$-PC and LiFSI-PC are more easily to arrive diffusion-controlled stage. **Fig. 2.6 (f-i)** are the same electrolytes above, but all of them are under the diffusion-controlled process. Lithium dendrites can grow in all the electrolytes under the diffusion-controlled process.

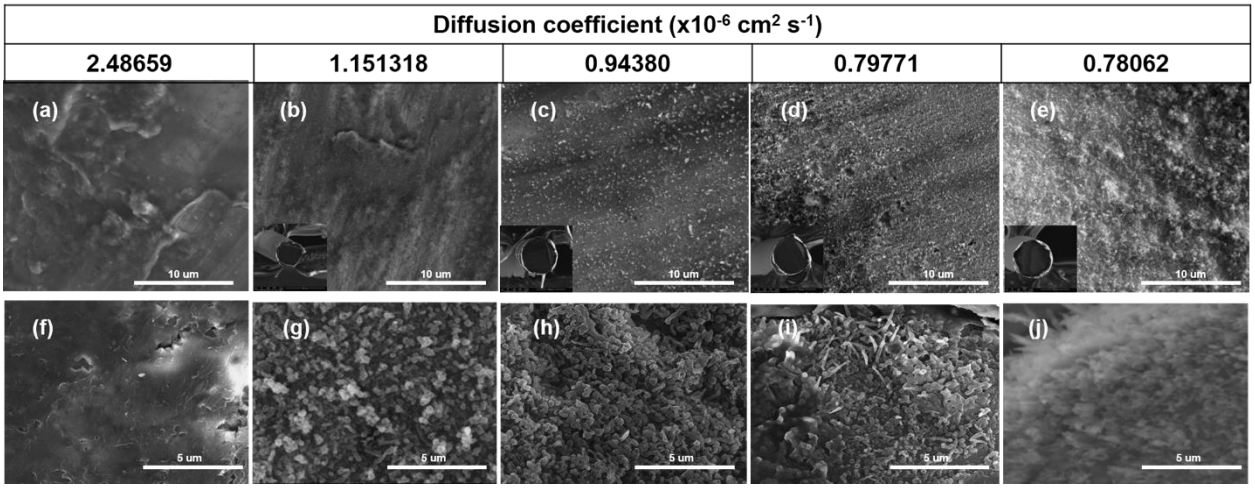

Figure 2.6 SEM images of lithium-ion deposition at 100 um micro-electrode in **(a)** 1.2 M LiFSI-TEP-BTFE, **(b)**1 M $LiPF_6$-PC, **(c)** 1 M LiTFSI-PC, **(d)** 1 M LiFSI-PC, and **(e)** 1 M $LiClO_4$-PC by LSV, potential step from 1 V to -0.35 V vs. Li^+/Li at 23℃ and scan rate is 20 mV s^{-1}. **(f)-(j)** are the SEM images in the diffusion control state.

2.3.2 Methods to study factors of diffusion coefficient and these factors for lithium deposit morphologies

Now that the fundamental factors impacting the ion transport and electrochemical reaction rate are studied along with the electrochemical tools to measure those key parameters, as a different approach. Then it can be proposed to tailor the aforementioned physical parameters which intrinsically alter the balance of mass transport and reaction rate. Moreover, the deposited morphologies of lithium.

As we mentioned above, the Stokes-Einstein equation describes the factors which can influence the diffusion coefficient. [42]

$$D = \frac{k_B T}{6\pi\eta r} \qquad (2)$$

Where, k_B is Boltzmann constant, T is temperature, η is the viscosity, and r is ionic radii. If the temperature is increased, the viscosity of the electrolytes will decrease, and then the diffusion coefficient can increase. On the other hand, if we keep constant temperature but increase the concentration, the diffusion coefficient will decrease due to increasing the viscosity. Here, these two factors are related to the diffusion coefficient, temperature and viscosity (influenced by concentration) and how they influence the lithium deposit morphologies.

Temperature influence

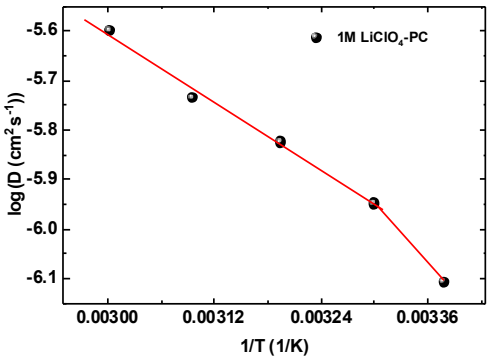

Figure 2.7 Diffusion coefficient by 25 um micro-electrode with chronoamperometry at different temperature in 1M $LiClO_4$-PC.

The Arrhenius plot of the diffusion coefficient is shown in **Fig. 2.7**. The data is a linear relationship between ln(D) and 1/T when the temperature is higher than 23℃. However, at 23℃, there is a step decreasing of diffusion coefficient. According to Wang et al.'s work, this phenomenon is also found in polymer electrolytes, which might be related to conductivity decreasing when the temperature becomes lower. [3, 43-46] The SEM images in **Fig. 2.8** show the lithium dendrites change with the diffusion coefficient due to the change of temperature. The

dendrite diameters become thicker at a higher temperature which is more safety because the thin diameter dendrites can pierce the membrane more easily, causing a short circuit. This also exposes more lithium to consume electrolytes due to the high surface area.

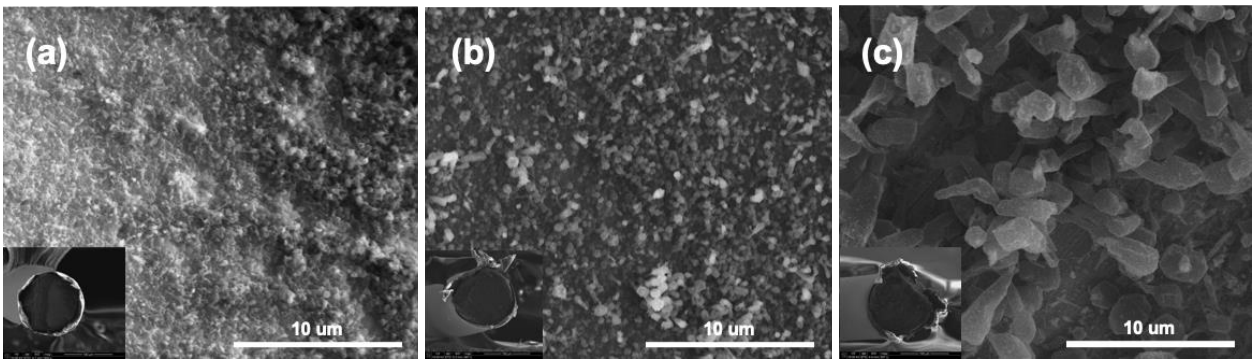

Figure 2.8 SEM images lithium-ion deposition at 100 um micro-electrode by LSV in 1 M $LiClO_4$-PC, potential step from 1 V to -0.35 V vs. Li^+/Li at **(a)** 23℃, **(b)** 30℃, and **(c)** 50℃, and the scan rate is 20 mV s^{-1}.

Concentration influences

The increasing concentration of lithium ions can increase the viscosity under the constant temperature. According to the Stokes-Einstein equation, increased viscosity can further decrease the diffusion coefficient. Increasing concentration can also mitigate the concentration gradient established in the vicinity of the electrode surfaces and thus alleviate the generation of dendritic Li. Therefore, a high concentration with minimum viscosity is desired to have both fast ion movement and a smoothed concentration gradient. In other words, it is not the higher the concentration, the better. There is a balanced or optimized concentrated range for each different electrolyte. As SEM images are shown in **Fig. 2.9**, the diameter of the lithium dendrites becomes smaller due to the diffusion coefficient decreases with concentration increasing. It is consistent

with the trend we found when we compared various electrolytes and temperature. The particle size of 4 M $LiClO_4$ in PC is larger than others (**Fig. 2.9 (d) & (h)**). That is because, in this test condition, the concentration is higher than others, but the viscosity is too large for lithium-ion diffusion. So, there are the thin rod-like lithium dendrites (yellow arrows) formed in a diffusion-controlled stage with diameter smaller than others.

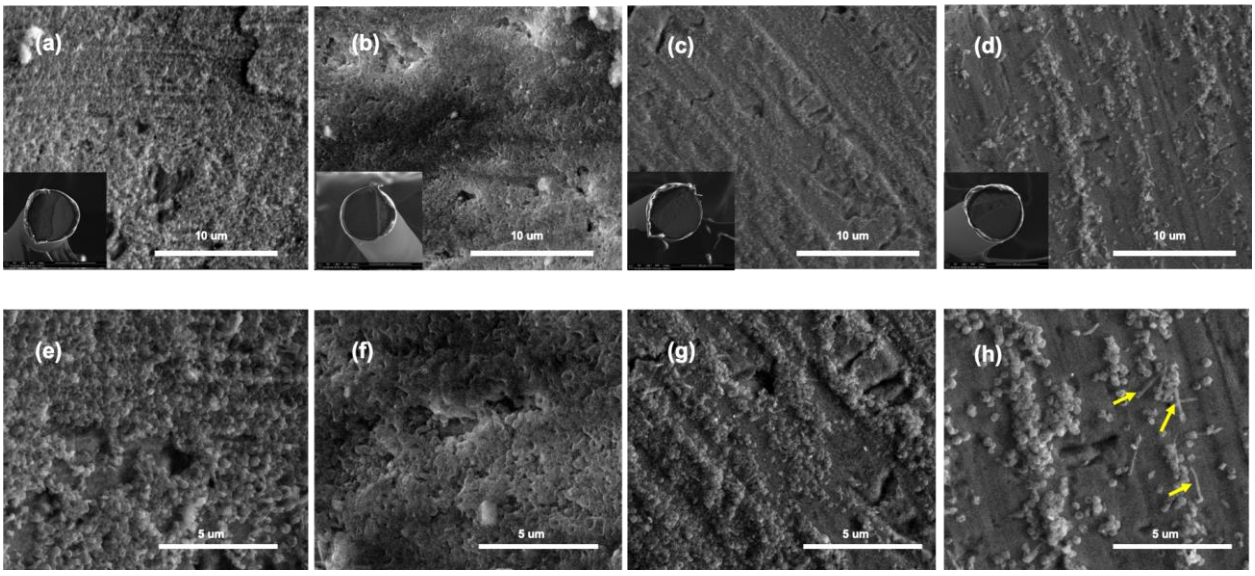

Figure 2.9 SEM images of lithium-ion deposition at 125 um Ni micro-electrode at different concentration **(a)** and **(e)** 0.5 M, **(b)** and **(f)**1.5 M, **(c)** and **(g)** 2 M, **(d)** and **(h)** 4 M $LiClO_4$-PC by LSV, potential step from 1 V to -0.35 V vs. Li^+/Li at 23℃ and scan rate is 20 mV s^{-1}.

2.4 Summary

The current distribution is usually not uniform due to the convection and electrode surface morphologies. In our situation, the diffusion-controlled process can happen in the local area, even in a short time, which is less than Sand's time at micro-electrodes, which is the beneficial property to apply micro-electrodes.

The diffusion coefficient is a critical parameter in the selection of electrolytes for lithium metal anode. The diffusion coefficients are decided by temperature, concentration, and the nature of molecules composing the electrolytes. So far, among all the electrolytes investigated, 1.2 M LiFSI in TEP-BTFE (1:3) was reported by Shuren Chen et al. which has very high diffusion coefficient 2.487 cm^2 s^{-1} and low viscosity shows the best performance for lithium metal anodes. The chemical-stable electrolytes that possess higher diffusion coefficient need to be investigated.

3 BENZENE-BASED ELECTROLYTES FOR LITHIUM METAL ANODES

The lithium metal anode which has the highest capacity (3860 mAh g^{-1}) and relatively lower potential (-3.04 V vs. SHE) is one of the most critical parts for lithium-sulfur batteries. However, lithium metal anodes are still facing enormous challenges for practical application, which massively hinders the development of lithium-sulfur batteries. On the one hand, the electrochemical potential of lithium metal is lower than most of the solvents which is responsible for solid electrolyte interface (SEI) formation and the progressive decrease of the Coulombic efficiency of the lithium metal anode during cycling. On the other hand, non-uniform lithium deposition induces dendritic growth, which exposes additional fresh lithium to the electrolyte, further leading to the consumption of the electrolyte. More state of art electrolytes needs to develop to meet the requirement of lithium metal batteries.

3.1 The potential of benzene as co-solvents of electrolytes

Benzene (PhH), (**Fig 3.1**), has a lower electrochemical potential (-3.18 V vs. SHE) than lithium metal which means that it is sufficient to suppress the side-reactions and remains stable in the presence of lithium metal when the overpotential is lower than ca.140 mV. Fresh bare lithium was immersed in pure benzene for 14 days, and the surface of the lithium plate was still like fresh lithium metal (shown in **Fig 3.1 (b)**), which indicating the lithium metal is contact stable in benzene.

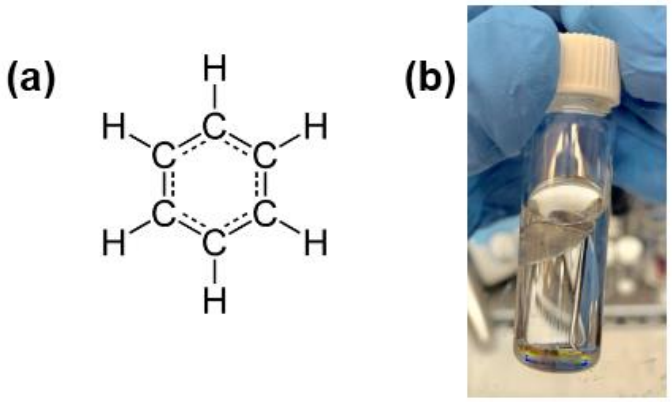

Figure 3.1 (a) Benzene chemical structure; **(b)** Lithium metal soaked in benzene for 14 days.

Benzene is a non-polar liquid, and therefore lithium salts do not dissolve in pure benzene. In the last decade, lithium-sulfur batteries have been thoroughly studied using ether-based electrolytes such as dioxolane (DOL) and dimethoxyethane (DME) mixture, and literature reveals that the mixture of DOL and DME possesses the best performance for lithium-sulfur batteries to date. By mixing benzene with these ether-based solvents at different volume ratios a class of new and novel benzene-ether based electrolytes were synthesized and tested for the compatibility with the Li-metal anode, as well as cycling stability and performance in Li-Cu half cells.

3.2 Results and discussion

Many common solvents which are compatible with graphite anodes are mixed with benzene, forming electrolytes. These mixed electrolytes are evaluated in Li-Cu half cells by Coulombic efficiency and cycle numbers.

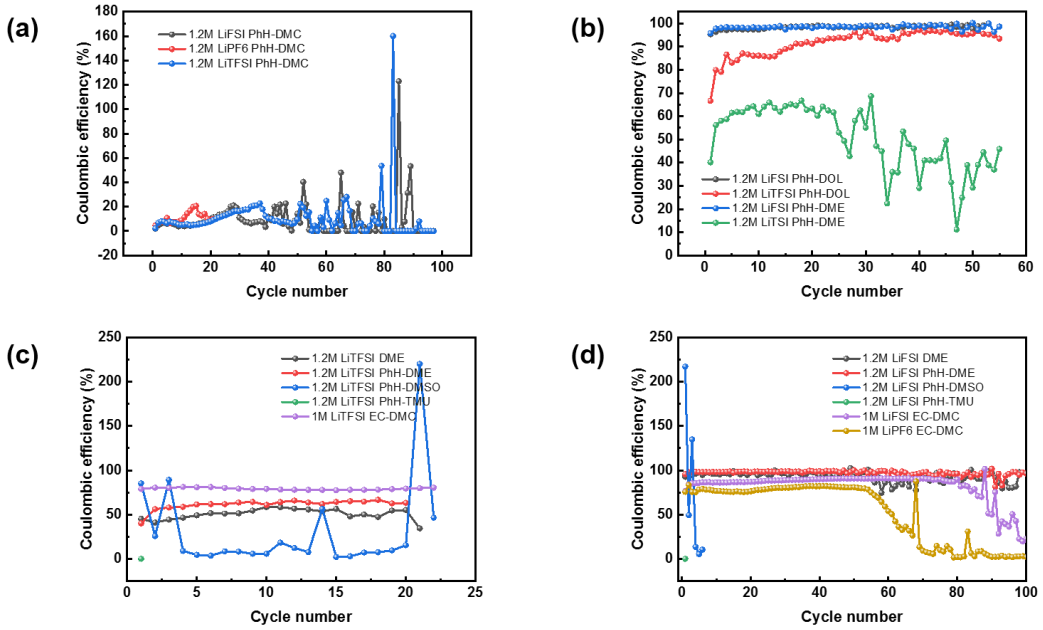

Figure 3.2 Li-Cu Coulombic efficiency performance in electrolytes of benzene mixed with **(a)** DMC and LiFSI as lithium salts, **(b)** DOL, DME, and LiFSI as lithium salts as well, **(c)** DMSO, TMU, and LiTFSI as lithium salts, **(d)** DMSO, TMU, and LiFSI as lithium salts.

Benzene mixed ethers, with LiSFI as the lithium salt, shows the best Coulombic efficiency and lifespan in **Fig 3.2 (b)**. Benzene mixed with other solvents such as esters, TMU, and DMSO as electrolytes are not compatible with the lithium metal anode. The best lithium salt for benzene-based electrolytes is LiFSI which achieves the highest Coulombic efficiency. For example, the Coulombic efficiency is higher than 98% in 1.2 M LiFSI PhH-DME within 50 cycles while deposition of lithium on Cu substrate cannot strip in 1.2 M LiFSI PhH-DMC. The reason might be the diverse solvation structure of lithium-ion in various types of organic solvents, leading to various reduced potential and SEI components. Notwithstanding, this still needs more spectroscopy characterization to demonstrate.

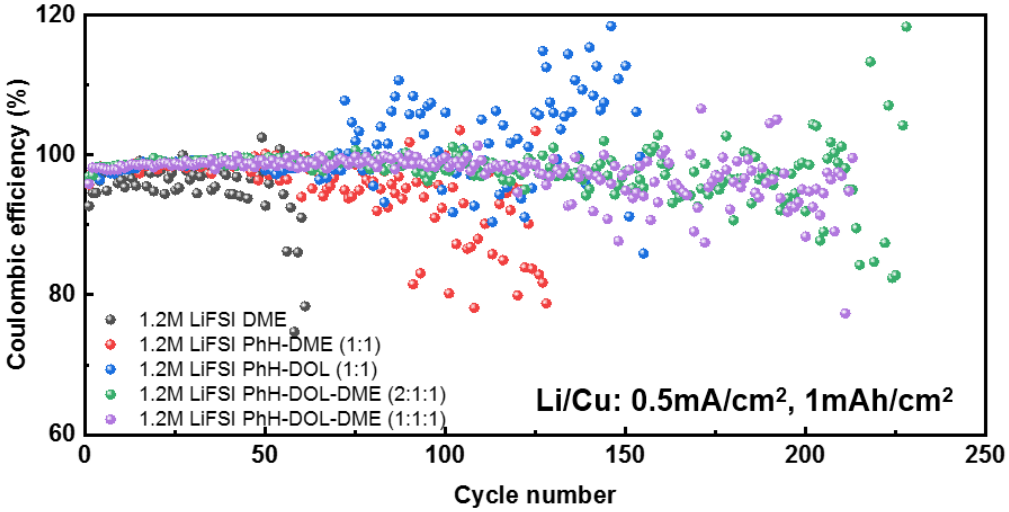

Figure 3.3 Coulombic efficiency of Li-Cu half cells used various electrolytes.

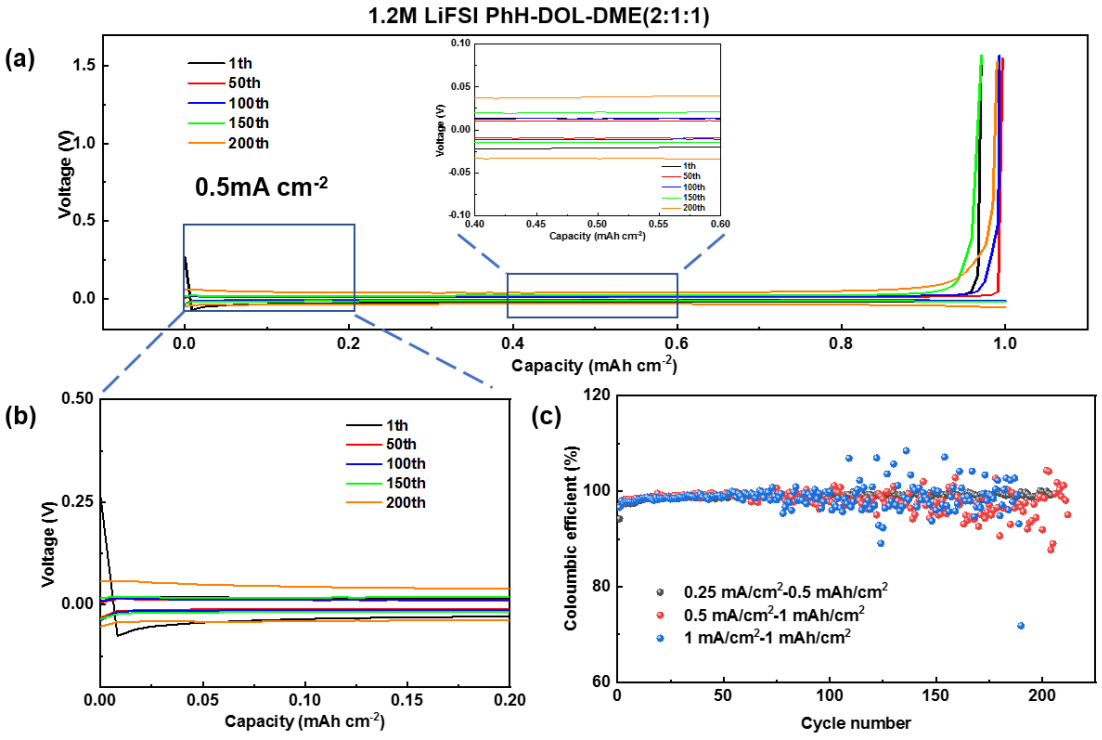

Figure 3.4 (a) and **(b)** Voltage profiles of 1.2 M LiFSI PhH-DOL-DME (2:1:1). **(c)** Coulombic efficiency of 1.2 M LiFSI PhH-DOL-DME (2:1:1) under various current density.

As indicated in **Fig. 3.4**, 1.2 M LiFSI PhH-DOL-DME (2:1:1) results in little polarization up to 200 cycles (**Fig. 3.4(a)**), and stable cycling from low to high current densities (**Fig. 3.4 (c)**). To determine that benzene is quite compatible with lithium metal anode, the coin cells are assembled, and the results are shown in **Fig 3.3**. It was found that the Coulombic efficiency of Li-Cu coin cells increased from ca. 95% to 99% when benzene is added in DME with a volume ratio of 1:1. Benzene mixed with DOL and DME shows the best performance when 1.2 M LiFSI is used as the lithium salt (**Fig. 3.3**).

Table 1. Diffusion coefficients of benzene-based electrolytes.

Solvent	**Lithium salt**	**Diffusion coefficient ($x10^{-6}$ cm^2 s^{-1})**
DME	1.2 M LiFSI	2.64
PhH-DME (1:1)	1.2 M LiFSI	1.94
PhH-DOL-DME (2:1:1)	1.2 M LiFSI	1.60

As illustrated in chapter 2, the diffusion coefficients significantly affect the deposition morphologies of lithium metal anodes. The diffusion coefficients of ether solution with benzene as co-solvent are under the order, 1.2 M LiFSI DME > 1.2 M LiFSI PhH-DME > 1.2 M LiFSI PhH-DOL-DME. The plated lithium morphologies at the micro-electrodes are shown in **Fig 3.5**. The diameter of dendrites in DME are thicker than the ones with benzene, which obeys the trend we found in the last chapter.

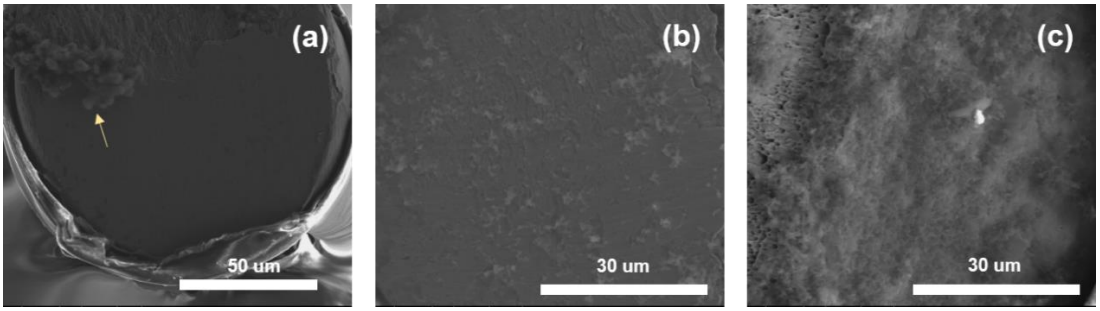

Figure 3.5 SEM of Micro-electrode tip with diameter of 125 um. Lithium deposited in **(a)** 1.2 M LiFSI DME, **(b)** 1.2 M LiFSI PhH-DME, and **(c)** 1.2 M LiFSI PhH-DOL-DME. The scan rate is 0.1 mV/s and the scan range is from 1 V to -0.3 V.

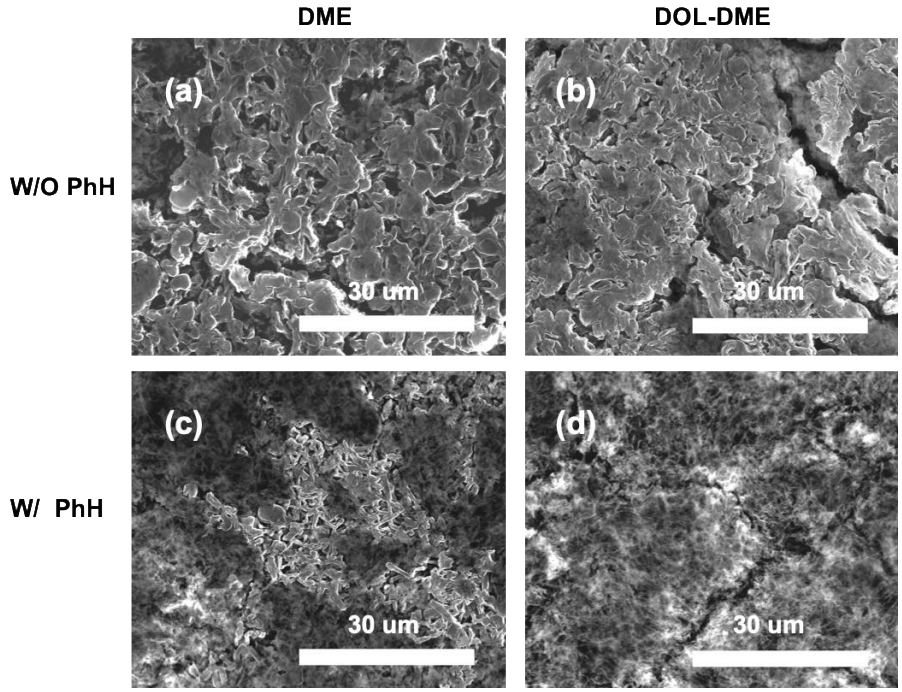

Figure 3.6 SEM images of lithium metal anodes after 10 cycles in contracting electrolytes with 1.2 M LiFSI.

The SEM images of the lithium metal anode morphologies after ten cycles of plating/stripping are shown in **Fig 3.6.** The surfaces of electrolytes with benzene show more compact lithium deposition, although PhH-DME and PhH-DOL-DME solvents show thinner dendrites.

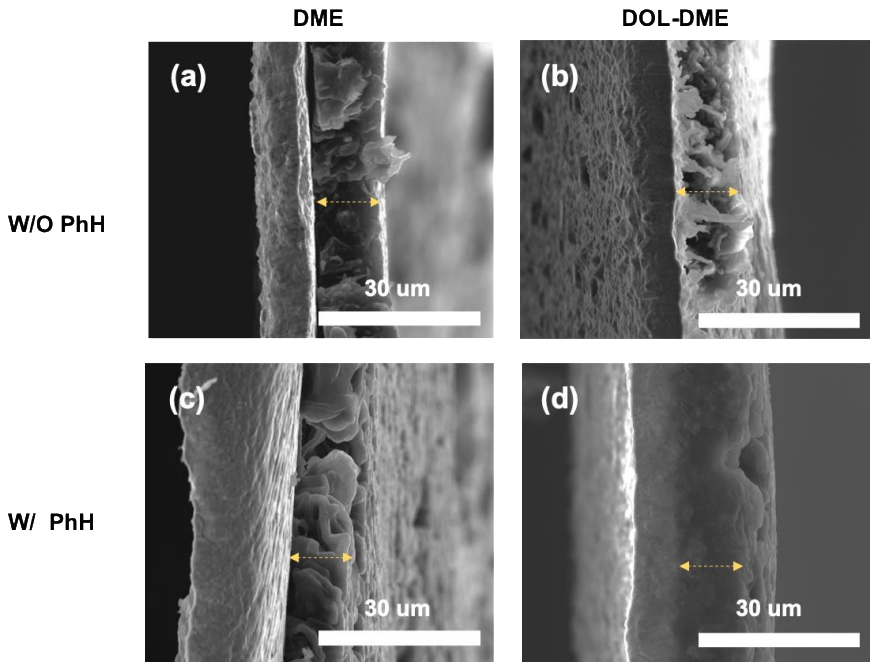

Figure 3.7 Cross-side of the first cycle lithium deposition on Cu substrates with and without benzene respectively.

The cross-section SEM images of the lithium deposition on the Cu substrate are shown in **Fig 3.7**. The lithium metal deposition in DME is denser than others, related to the higher diffusion coefficient, which results in more even deposition. Thinner dendrites grow in benzene-based electrolytes, although the final performance of electrolytes with benzene is better than that of the same electrolytes without it. That means dendrite growth is not the only factor to impact the performance of lithium metal anodes and SEI might be another critical impactor. To determine the solvent influences on SEI, which are related to the stability and electrochemical properties of lithium metal anode, XPS is employed to identify the components on the electrode substrates. Cu is applied as a substrate to deposit lithium and charge/discharge after ten cycles, receiving a reliable SEI which occurs in a practical situation.

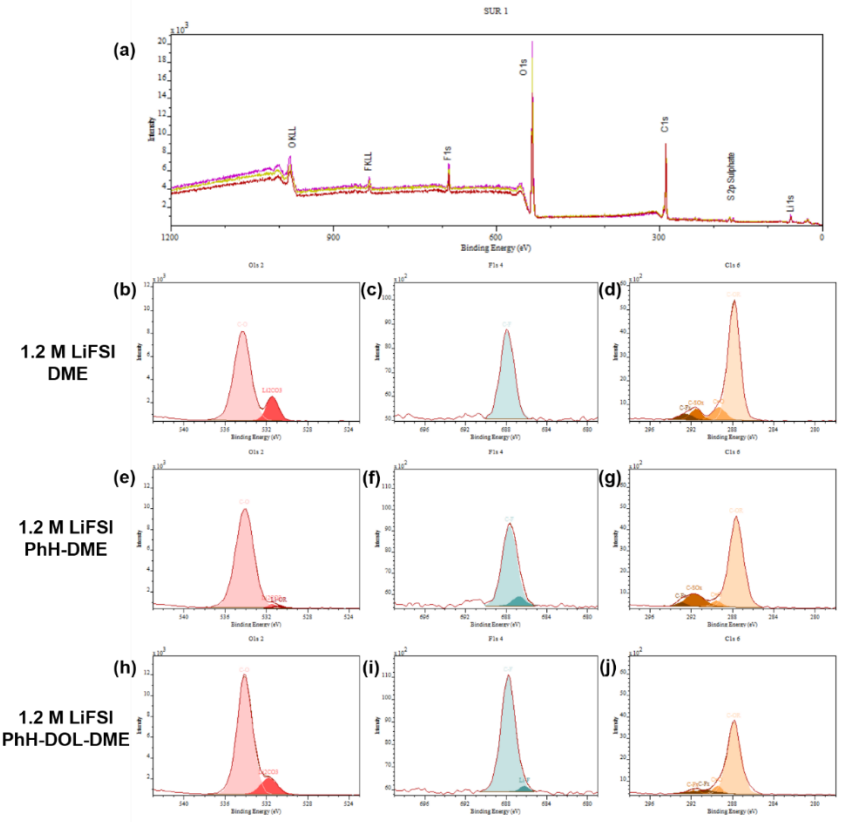

Figure 3.8 XPS of lithium metal deposition after 10cycles at Cu substrates in different solvents of **(b, c, d)** DME, **(e, f, g)** PhH-DME (1:1), and **(h, i, j)** PhH-DOL-DME (2:1:1).

XPS was used to analyze the element content and valence on the surface of these Li anodes. The surface of the lithium contains elements of C, O, F, and S. [47-49] In the O 1s spectroscopy, the products at the lithium metal anodes such as C-O (53.4.3 eV) and Li_2CO_3 (531.4 eV) are different. The ratio of Li_2CO_3 in the SEI decreases when adding benzene as a co-solvent in 1.2 M LiFSI DME, which remains steady and presents effective protection to alleviate the corrosion effect of electrolyte. However, if DOL is continually added to 1.2 M LiFSI PhH-DME, the peak of Li_2CO_3 increases back again due to decomposition of DOL and forming the more robust SEI. There are more C-F (687.9 eV) in PhH-DOL-DME than in the other two electrolytes in F 1s

spectroscopy, which are desirable components for SEI. As shown in C 1s spectroscopy, more C-SOx (291.5 eV) from FSI^- is observed in PhH-DME than other two electrolytes, which means more anions are decomposed even though benzene can reduce the reaction between lithium metal and DME. The components of Li_2CO_3 (289.3 eV) retain a similar trend with O 1s spectroscopy. Thus, the DOL can form a better SEI which can prevent anions from decomposing.

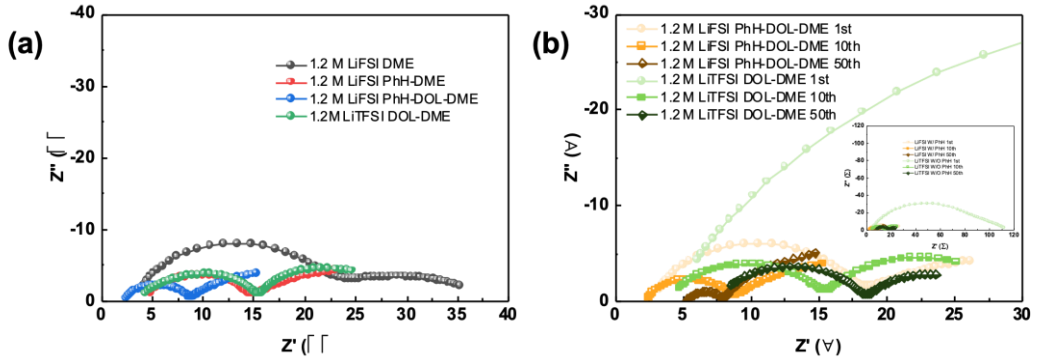

Figure 3.9 Impedance of Li | Li symmetric coin cells **(a)** in different electrolytes at 10cycles, and **(b)** in 1.2 M LiFSI PhH-DOL-DME and 1.2 M LiTFSI DOL-DME at different cycles respectively.

After several cycles of charge and discharge processes, the dead lithium induced by lithium dendrite accumulates on the surface of lithium metal electrodes, which causes the impedances of the cells to increase and leads to battery failure eventually. The impedance of various electrolytes at 10^{th} cycle is shown in **Fig 3.9 (a)**. The 1.2 M LiFSI PhH-DOL-DME offers the lowest impedance among these electrolytes, including the most accepted electrolyte in Li-S batteries (1.2 M LiTFSI DOL-DME). The impedance at various cycles are compared in **Fig 3.9 (b)**, where it is evident that the impedance of 1.2 M LiFSI PhH-DOL-DME is lower than 1.2 M LiTFSI

DOL-DME at every cycle, and the impedance of benzene-based electrolyte is decreasing with cycling within 50 cycles, unlike 1.2 M LiTSI DOL-DME which first drops then rises.

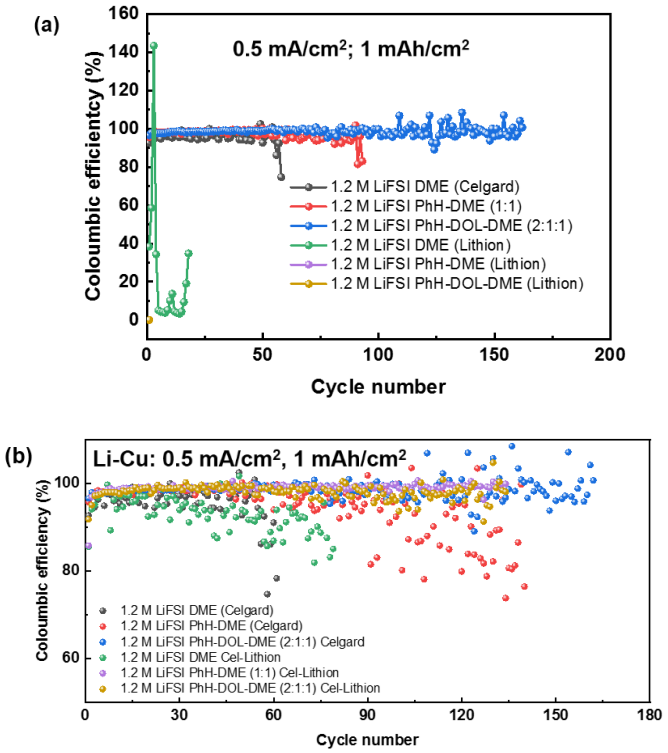

Figure 3.10 (a) Coulombic efficiencies of various electrolytes employing Lithion self-standing membranes as separators. **(b)** Coulombic efficiencies of various electrolytes employing Lithion coated membranes as separators.

The developed new benzene-based electrolytes are entirely compatible with lithium metal anodes, and it was found that1.2 M LiFSI in PhH-DOL-DME (2:1:1) shows the best performance in terms of Coulombic efficiency, as well as a low and relatively stable overpotential. Furthermore, the best benzene-based electrolyte was used in conjunction with Lithion, and Lithion coated Celgard membranes as separators (provided by Giner). It was found that Lithion coated Celgard has better performance than Celgard alone.

Concentrated electrolytes have been explored to stabilize lithium metal anode due to the typical solvation of solvent molecules with lithium ions, which is called “salts in solvents”. The Coulombic efficiencies of benzene-based concentrated electrolytes are determined by coin cells as well. The 4 M LiFSI Li-Cu cells have the most stability (lasting 150 cycles), and highest Coulombic efficiency at above 99% in both PhH-DME and PhH-DOL-DME. PhH-DME (1:1) with 4 M LiFSI is most compatible with lithium metal anodes as shown in **Fig. 3.11**.

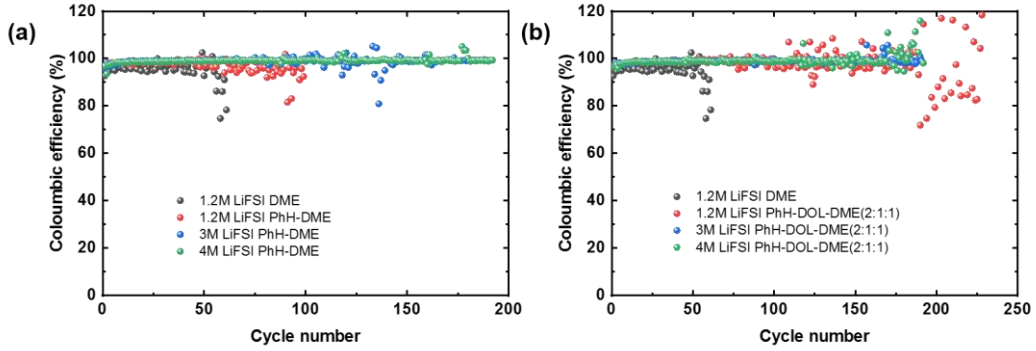

Figure 3.11 Coulombic efficiencies of Li-Cu coin cells in **(a)** PhH-DME electrolytes and **(b)** PhH-DOL-DME electrolytes with various lithium salt concentration at 0.5 mA cm^{-2} and 1 mAh cm^{-2}.

3.3 Summary

The benzene-based solvents show high compatible properties with lithium metal anodes as co-solvent in electrolytes due to the low reduction potential. The best benzene-based electrolyte is 1.2 M LiFSI PhH-DOL-DME, which has shown to have Coulombic efficiency greater than 99% in the Li-Cu coin cells and the lowest impedance in Li-Li symmetric cells. This electrolyte can be applied at high rate charge and discharge conditions. The diffusion coefficients of benzene-

based electrolytes are relatively lower than the one without benzene, which leads to thinner dendrites growth, although the performances in the coin cells are better than the one without benzene. However, the benzene-based electrolytes are more chemically stable with lithium metal due to the lower electrochemical potential. Thus, this new type of electrolytes can potentially be used in lithium-sulfur and other lithium metal batteries.

4 BENZENE-BASED ELELCTROLYTES FOR LITHIUM METAL BATTERIES

4.1 Background

The benzene-base solvents were demonstrated to be compatible with lithium metal anode in the last chapter. In this chapter, sulfur cathodes and NCM cathodes are used to assemble coin cells with benzene-based electrolytes.

Li-ion batteries are reaching their theoretical capacity limit, while the demands for lower price and higher energy density are still increasing. Lithium metal batteries are the promising next-generation energy store system such as Li-Sulfur batteries [7, 15, 16, 43, 50-55] and NCM cathodes [5, 8, 56, 57] with lithium metal as anodes. Thus, it is significant to investigate the performance of benzene-based electrolytes in both these battery systems.

4.2 Results and discussion

Lithium-Sulfur full coin cells are assembled with benzene-based electrolytes which are then compared with the most common electrolyte used in Li-S batteries (1 M LiTFSI + 0.2 M $LiNO_3$ DOL-DME). Of the benzene-based electrolytes, it was found that 1 M LiFSI + 0.2 M $LiNO_3$ PhH-DOL-DME (2:1:1 by volume) is the most compatible with lithium metal anode. As shown in **Fig 4.1 (a)**, the capacities in both electrolytes are similar for the first 10 cycles. After that, the capacities of the cells using benzene-base electrolyte are lower than non-benzene electrolyte, but the discharge capacities are both keeping stable within 100 cycles at 0.2 C. When the charging/discharging rates increase to 0.5 C, the capacities of each cell is decreasing. The

capacities of electrolytes with benzene decrease significantly after 80 cycles as shown in **Fig. 4.1 (b)**.

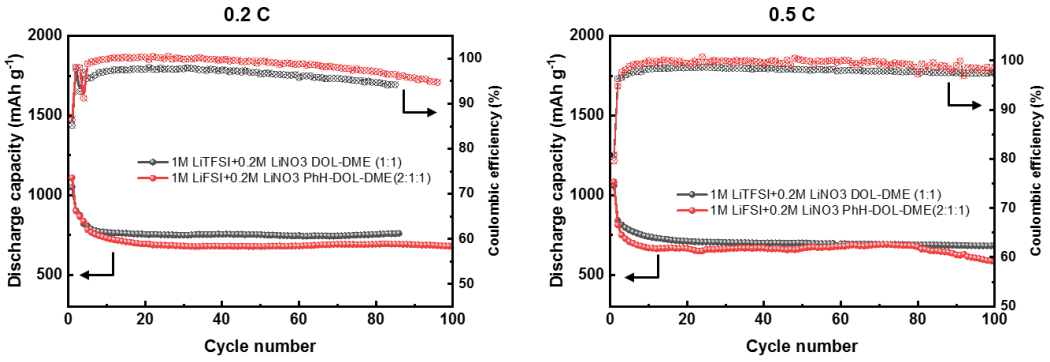

Figure 4.1 (a) Discharge capacity and Coulombic efficiency of Li-S coin cells at 0.2 C; **(b)** voltage profiles of Li-S coin cells with 1 M LiFSI + 0.2 M $LiNO_3$ PhH-DOL-DME (2:1:1) as electrolyte at 0.2 C.

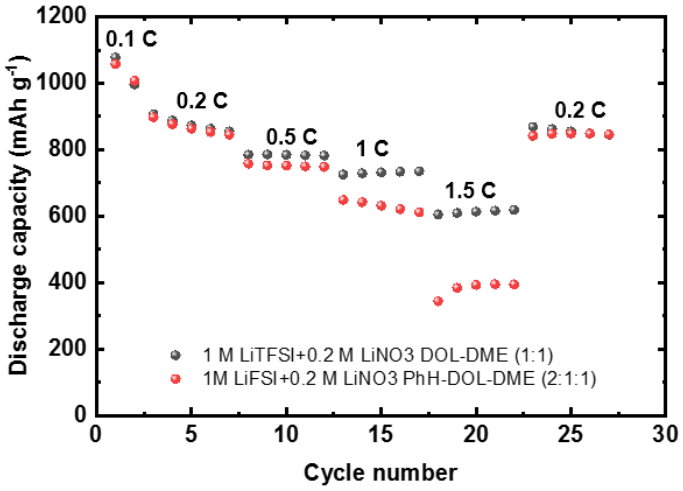

Figure 4.2 Discharge capacity of different rates for two electrolytes

Various charging/discharging rates were applied to the coin cells in both electrolytes. The specific discharge capacities of coin cells using 1 M LiFSI + 0.2 M $LiNO_3$ PhH-DOl-DME as electrolyte are similar with the electrolytes without benzene at low current density (0.2 C) within

the first 5 cycles. Once the current densities are increased, the performances with benzene become worse than the one without benzene. Specifically, at a high rate (1.5 C), the capacities of cells with benzene electrolytes is only half the capacities achieved at low rate cycling (0.2 C). When the cycling current density decreases back to 0.2 C, the capacities of both electrolytes become similar again. The results of discharge capacity performances might be related to anions because FSI^- can react with polysulfides.

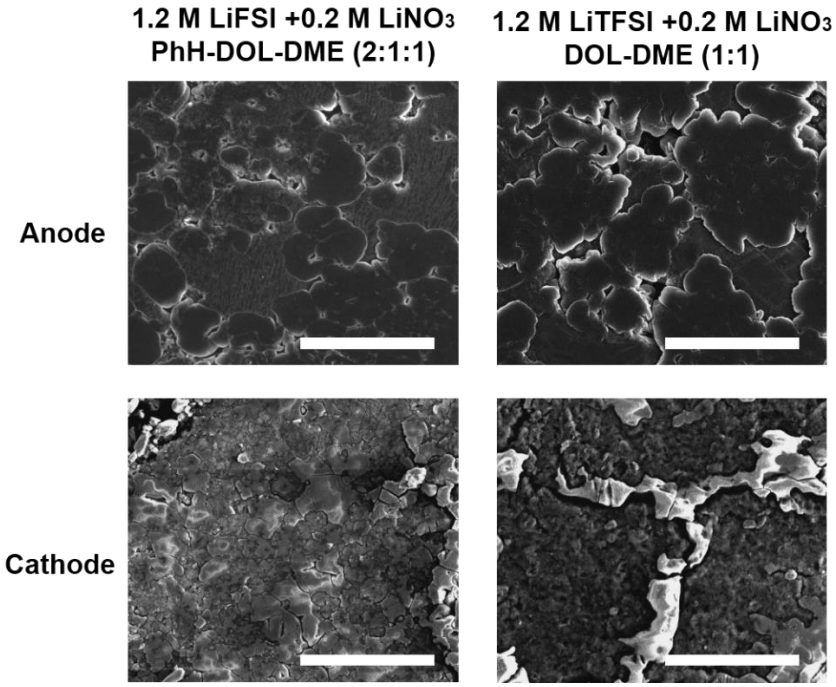

Figure 4.3 SEM images of anodes and cathodes in two different electrolytes. The scale bar is 100 um.

From the SEM images of the lithium metal anodes from both cells (**Fig. 4.3**), it can be seen that the lithium deposition formed island shapes. The lithium deposition in electrolytes with benzene formed smaller islands than the one in electrolytes without benzene, which means that the lithium plating is more uniform when benzene is used as a co-solvent.

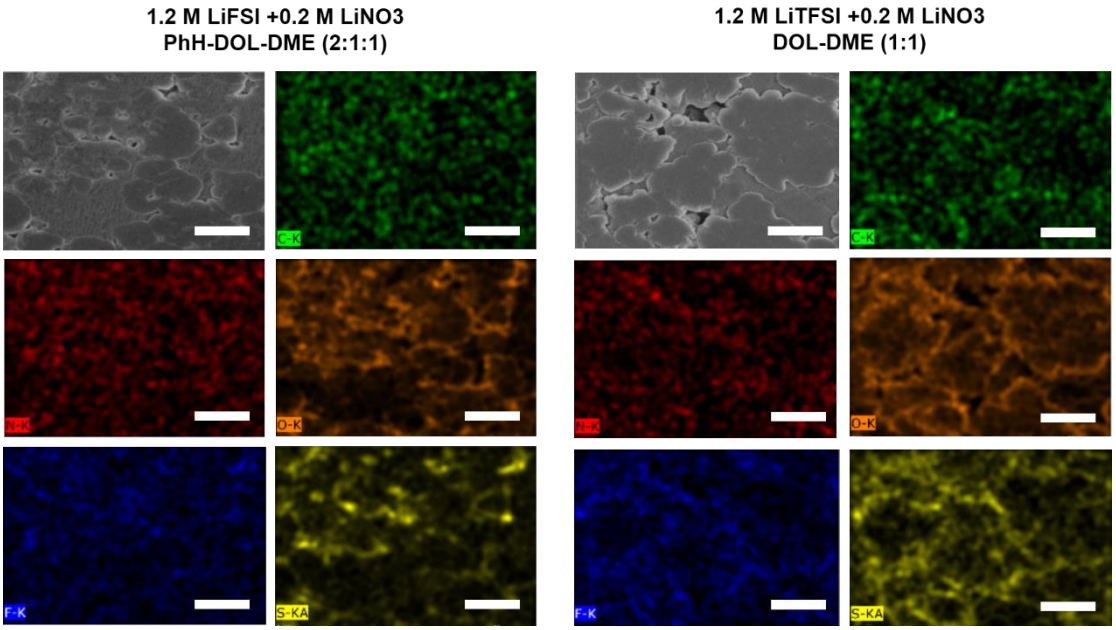

Figure 4.4 SEM and EDX of anodes from electrolytes **(a)** with benzene, **(b)** without benzene, respectively. The scale bar is 50 um.

The anodes after cycling in lithium-sulfur batteries become more complicated to investigate due to the polysulfides. Here, SEM and EDX are combined to investigate the components on the surface of anodes. As shown in **Fig 4.4**, the elemental maps of carbon, nitrogen, as well as fluoride are very similar between two electrolytes. The O element appears at the edges of lithium deposition islands. The distribution of O is different between two electrolytes due to the various size of lithium plating islands. The lithium metal islands become smaller when benzene as co-solvent, so the distribution of O is more uniform. The S element is from polysulfides, and it is easier to accumulate in porous structures on the surface. Thus, there are fewer polysulfides on the surface of lithium metal when the electrolyte contains benzene. The elements distribution cannot be distinguished on the cathodes between two electrolytes, as shown in **Fig 4.5**.

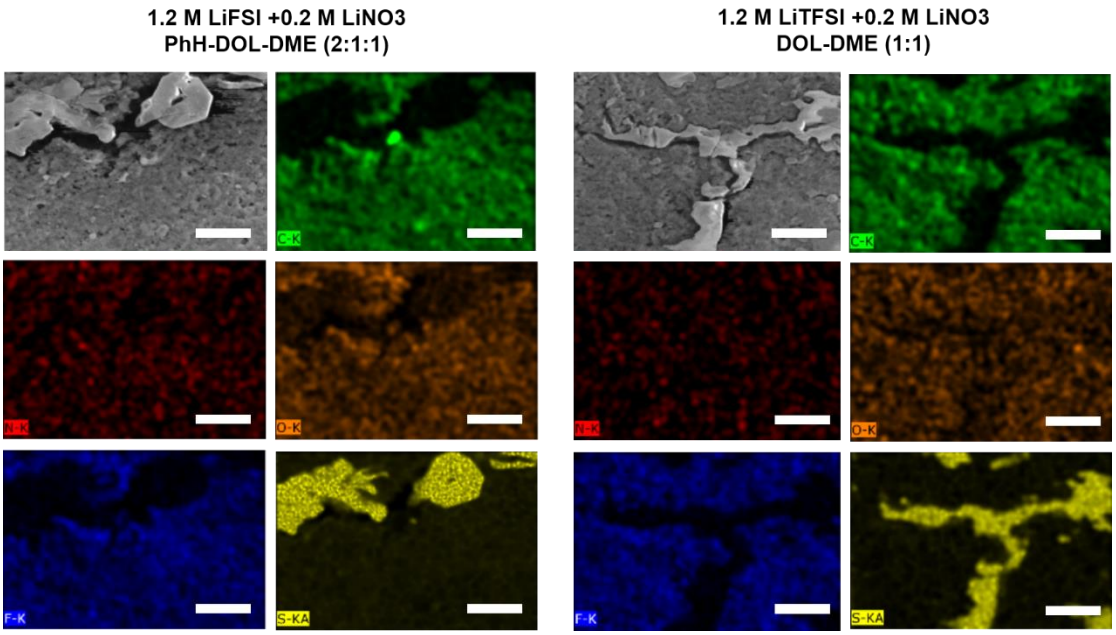

Figure 4.5 SEM and EDX of anodes from electrolytes **(a)** with benzene, **(b)** without benzene, respectively. The scale bar is 50 um.

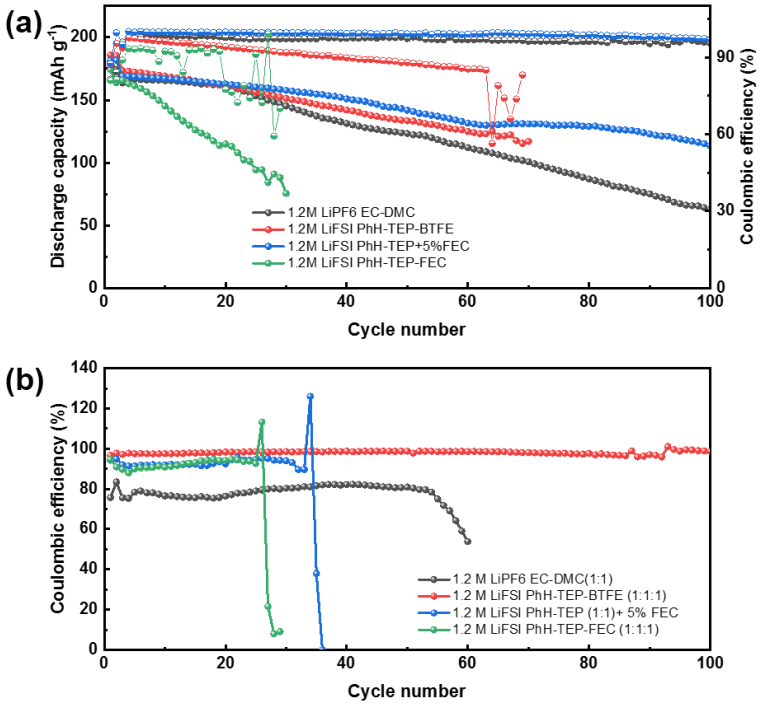

Figure 4.6 (a) Discharge capacity and Coulombic efficiencies of NCM (622) full coin cells, **(b)** Coulomibc efficiencies of Li-Cu half coin cells used the same electrolytes.

The performance of benzene-base electrolytes in NCM coin cells are shown in **Fig 4.6 (a)**. The best one is 1.2 M LIFSI PhH-TEP + 5% FEC. However, if the FEC ratio is increased to one third (PhH-TEP-FEC: 1:1:1 by volume), the capacities decrease very fast. One of the reasons is that this ratio of electrolyte is not stable with lithium metal anode (shown in **Fig 4.6 (b)**), and it can form the high impedance SEI. 1.2 M LiFSI PhH-TEP-BTFE results in a high Coulombic efficiency in the Li-Cu coin cells, which means that this electrolyte is compatible with lithium metal. However, the Coulombic efficiencies of NCM full cells decrease very fast after 60 cycles resulting in quicker failure of the cells.

4.3 Summary

The benzene-based electrolytes can be used in lithium metal batteries, although more co-solvents need to develop to be compatible with different cathodes. So far, among the electrolytes with benzene as a co-solvent, for lithium-sulfur batteries, 1 M LiFSI + 0.2 M $LiNO_3$ PhH-DOL-DME (2:1:1 by volume) is the best electrolyte. And 1.2 M LiFSI PhH-TEP + 5% FEC is the best electrolyte for NCM cathodes, even though this electrolyte is not compatible with lithium metal anode at relatively high current density.

5 CONCLUSION

In this work, the kinetic parameters of electrolytes are determined, and the effects of these parameters on lithium metal, as well as anode electro-plating micro-structures, are also investigated. At the similar exchange current density, the higher diffusion coefficient of the electrolytes, lithium deposition becomes more uniform. The diffusion coefficient is defined by the Stoke-Einstein equation, which includes the parameters such as temperature, concentration, viscosity, as well as the solvated ion radius. The relationships between the lithium electro-plating morphologies and these parameters are investigated.

After exploring the fundamental mechanics, benzene as a co-solvent is first time used in lithium metal batteries to adjust the ionic solvation structures for lithium metal protection. It was found that 1.2 M LiFSI PhH-DOL-DME (2:1:1) electrolyte shows the best Coulomibc efficiency in Li-Cu coin cells and the largest stable cycle number. Concentrated electrolytes were also explored, and the 4 M LiFSI PhH-DME electrolyte shows the excellent performance in coin cells, which can cycle more than 200 times, with Coulombic efficiency greater than 99%. 1 M LiFSI + 0.2 M $LiNO_3$ PhH-DOL-DME (2:1:1) are used in lithium-sulfur batteries which can cycle more than 100 times with capacity retention greater than 80%.

6 REFERENCES

[1] X. B. Cheng, R. Zhang, C. Z. Zhao, and Q. Zhang, "Toward Safe Lithium Metal Anode in Rechargeable Batteries: A Review," *Chemical Reviews,* vol. 117, no. 15, pp. 10403-10473, Aug 2017, doi: 10.1021/acs.chemrev.7b00115.

[2] Y. P. Guo, H. Q. Li, and T. Y. Zhai, "Reviving Lithium-Metal Anodes for Next-Generation High-Energy Batteries," *Advanced Materials,* vol. 29, no. 29, Aug 2017, Art no. 1700007, doi: 10.1002/adma.201700007.

[3] X. B. Cheng, R. Zhang, C. Z. Zhao, F. Wei, J. G. Zhang, and Q. Zhang, "A Review of Solid Electrolyte Interphases on Lithium Metal Anode," *Advanced Science,* vol. 3, no. 3, Mar 2016, Art no. Unsp 1500213, doi: 10.1002/advs.201500213.

[4] E. Peled and S. Menkin, "Review-SEI: Past, Present and Future," *Journal of the Electrochemical Society,* vol. 164, no. 7, pp. A1703-A1719, 2017, doi: 10.1149/2.1441707jes.

[5] N. Nitta, F. X. Wu, J. T. Lee, and G. Yushin, "Li-ion battery materials: present and future," *Materials Today,* vol. 18, no. 5, pp. 252-264, Jun 2015, doi: 10.1016/j.mattod.2014.10.040.

[6] R. Younesi, G. M. Veith, P. Johansson, K. Edstrom, and T. Vegge, "Lithium salts for advanced lithium batteries: Li-metal, Li-O-2, and Li-S," *Energy & Environmental Science,* vol. 8, no. 7, pp. 1905-1922, 2015, doi: 10.1039/c5ee01215e.

[7] H. J. Peng, J. Q. Huang, X. B. Cheng, and Q. Zhang, "Review on High-Loading and High-Energy Lithium-Sulfur Batteries," *Advanced Energy Materials,* vol. 7, no. 24, Dec 2017, Art no. 1700260, doi: 10.1002/aenm.201700260.

[8] X. B. Cheng *et al.*, "Implantable Solid Electrolyte Interphase in Lithium-Metal Batteries," *Chem,* vol. 2, no. 2, pp. 258-270, Feb 2017, doi: 10.1016/j.chempr.2017.01.003.

[9] Q. W. Lu *et al.*, "Dendrite-Free, High-Rate, Long-Life Lithium Metal Batteries with a 3D Cross-Linked Network Polymer Electrolyte," *Advanced Materials,* vol. 29, no. 13, Apr 2017, Art no. 1604460, doi: 10.1002/adma.201604460.

[10] X. B. Cheng *et al.*, "Dendrite-Free Lithium Deposition Induced by Uniformly Distributed Lithium Ions for Efficient Lithium Metal Batteries," *Advanced Materials,* vol. 28, no. 15, pp. 2888-2895, Apr 2016, doi: 10.1002/adma.201506124.

[11] Z. Li, J. Huang, B. Y. Liaw, V. Metzler, and J. B. Zhang, "A review of lithium deposition in lithium-ion and lithium metal secondary batteries," *Journal of Power Sources,* vol. 254, pp. 168-182, May 2014, doi: 10.1016/j.jpowsour.2013.12.099.

[12] G. Bieker, M. Winter, and P. Bieker, "Electrochemical in situ investigations of SEI and dendrite formation on the lithium metal anode," *Physical Chemistry Chemical Physics,* vol. 17, no. 14, pp. 8670-8679, 2015, doi: 10.1039/c4cp05865h.

[13] E. Peled, D. Golodnitsky, C. Menachem, and D. Bar-Tow, "An advanced tool for the selection of electrolyte components for rechargeable lithium batteries," *Journal of the Electrochemical Society,* vol. 145, no. 10, pp. 3482-3486, Oct 1998, doi: 10.1149/1.1838831.

[14] E. Peled, D. Golodnitsky, and G. Ardel, "Advanced model for solid electrolyte interphase electrodes in liquid and polymer electrolytes," *Journal of the Electrochemical Society,* vol. 144, no. 8, pp. L208-L210, Aug 1997, doi: 10.1149/1.1837858.

[15] Z. W. Seh, Y. M. Sun, Q. F. Zhang, and Y. Cui, "Designing high-energy lithium-sulfur batteries," *Chemical Society Reviews,* vol. 45, no. 20, pp. 5605-5634, 2016, doi: 10.1039/c5cs00410a.

[16] M. A. Pope and I. A. Aksay, "Structural Design of Cathodes for Li-S Batteries," *Advanced Energy Materials,* vol. 5, no. 16, Aug 2015, Art no. 1500124, doi: 10.1002/aenm.201500124.

[17] S. Y. Wei, L. Ma, K. E. Hendrickson, Z. Y. Tu, and L. A. Archer, "Metal-Sulfur Battery Cathodes Based on PAN Sulfur Composites," *Journal of the American Chemical Society,* vol. 137, no. 37, pp. 12143-12152, Sep 2015, doi: 10.1021/jacs.5b08113.

[18] Y. Yang, G. Y. Zheng, S. Misra, J. Nelson, M. F. Toney, and Y. Cui, "High-Capacity Micrometer-Sized Li2S Particles as Cathode Materials for Advanced Rechargeable Lithium-Ion Batteries," *Journal of the American Chemical Society,* vol. 134, no. 37, pp. 15387-15394, Sep 2012, doi: 10.1021/ja3052206.

[19] X. Q. Zhang, X. B. Cheng, X. Chen, C. Yan, and Q. Zhang, "Fluoroethylene Carbonate Additives to Render Uniform Li Deposits in Lithium Metal Batteries," *Advanced Functional Materials,* vol. 27, no. 10, Mar 2017, Art no. Unsp 1605989, doi: 10.1002/adfm.201605989.

[20] J. M. Zheng *et al.*, "Ionic liquid-enhanced solid state electrolyte interface (SEI) for lithium-sulfur batteries," *Journal of Materials Chemistry A,* vol. 1, no. 29, pp. 8464-8470, 2013, doi: 10.1039/c3ta11553d.

[21] J. B. Goodenough and Y. Kim, "Challenges for Rechargeable Li Batteries," *Chemistry of Materials,* vol. 22, no. 3, pp. 587-603, Feb 2010, doi: 10.1021/cm901452z.

[22] S. S. Zhang, "An unique lithium salt for the improved electrolyte of Li-ion battery," *Electrochemistry Communications,* vol. 8, no. 9, pp. 1423-1428, Sep 2006, doi: 10.1016/j.elecom.2006.06.016.

[23] T. Kawamura, A. Kimura, M. Egashira, S. Okada, and J. I. Yamaki, "Thermal stability of alkyl carbonate mixed-solvent electrolytes for lithium ion cells," *Journal of Power Sources,* vol. 104, no. 2, pp. 260-264, Feb 2002, Art no. Pii s0378-7753(01)00960-0, doi: 10.1016/s0378-7753(01)00960-0.

[24] J. Qin *et al.*, "Graphene Networks Anchored with Sn@Graphene as Lithium Ion Battery Anode," *Acs Nano,* vol. 8, no. 2, pp. 1728-1738, Feb 2014, doi: 10.1021/nn406105n.

[25] X. H. Cao *et al.*, "Preparation of MoS2-Coated Three-Dimensional Graphene Networks for High-Performance Anode Material in Lithium-Ion Batteries," *Small,* vol. 9, no. 20, pp. 3433-3438, Oct 2013, doi: 10.1002/smll.201202697.

[26] R. Schmuch, R. Wagner, G. Horpel, T. Placke, and M. Winter, "Performance and cost of materials for lithium-based rechargeable automotive batteries," *Nature Energy,* vol. 3, no. 4, pp. 267-278, Apr 2018, doi: 10.1038/s41560-018-0107-2.

[27] D. C. Lin, Y. Y. Liu, and Y. Cui, "Reviving the lithium metal anode for high-energy batteries," *Nature Nanotechnology,* vol. 12, no. 3, pp. 194-206, Mar 2017, doi: 10.1038/nnano.2017.16.

[28] X. G. Han *et al.*, "Negating interfacial impedance in garnet-based solid-state Li metal batteries," *Nature Materials,* vol. 16, no. 5, pp. 572-+, May 2017, doi: 10.1038/nmat4821.

[29] P. Bai, J. Li, F. R. Brushett, and M. Z. Bazant, "Transition of lithium growth mechanisms in liquid electrolytes," (in English), *Energy & Environmental Science,* Article vol. 9, no. 10, pp. 3221-3229, 2016, doi: 10.1039/c6ee01674j.

[30] M. S. Park, S. B. Ma, D. J. Lee, D. Im, S. G. Doo, and O. Yamamoto, "A Highly Reversible Lithium Metal Anode," *Scientific Reports,* vol. 4, Jan 2014, Art no. 3815, doi: 10.1038/srep03815.

[31] M. H. Ryou, D. J. Lee, J. N. Lee, Y. M. Lee, J. K. Park, and J. W. Choi, "Excellent Cycle Life of Lithium-Metal Anodes in Lithium-Ion Batteries with Mussel-Inspired Polydopamine-Coated Separators," *Advanced Energy Materials,* vol. 2, no. 6, pp. 645-650, Jun 2012, doi: 10.1002/aenm.201100687.

[32] S. S. Zhang and J. A. Read, "A new direction for the performance improvement of rechargeable lithium/sulfur batteries," *Journal of Power Sources,* vol. 200, pp. 77-82, Feb 2012, doi: 10.1016/j.jpowsour.2011.10.076.

[33] A. Zhamu *et al.*, "Reviving rechargeable lithium metal batteries: enabling next-generation high-energy and high-power cells," *Energy & Environmental Science,* vol. 5, no. 2, pp. 5701-5707, Feb 2012, doi: 10.1039/c2ee02911a.

[34] G. Girishkumar, B. McCloskey, A. C. Luntz, S. Swanson, and W. Wilcke, "Lithium - Air Battery: Promise and Challenges," *Journal of Physical Chemistry Letters,* vol. 1, no. 14, pp. 2193-2203, Jul 2010, doi: 10.1021/jz1005384.

[35] M. S. Chandrasekar and M. Pushpavanam, "Pulse and pulse reverse plating - Conceptual, advantages and applications," (in English), *Electrochimica Acta,* Review vol. 53, no. 8, pp. 3313-3322, Mar 2008, doi: 10.1016/j.electacta.2007.11.054.

[36] J. F. Qian *et al.*, "High rate and stable cycling of lithium metal anode," (in English), *Nature Communications,* Article vol. 6, p. 9, Feb 2015, Art no. 6362, doi: 10.1038/ncomms7362.

[37] X. Su, Q. L. Wu, X. Zhan, J. Wu, S. Y. Wei, and Z. H. Guo, "Advanced titania nanostructures and composites for lithium ion battery," *Journal of Materials Science,* vol. 47, no. 6, pp. 2519-2534, Mar 2012, doi: 10.1007/s10853-011-5974-x.

[38] D. Aurbach *et al.*, "Recent studies on the correlation between surface chemistry, morphology, three-dimensional structures and performance of Li and Li-C intercalation anodes in several important electrolyte systems," *Journal of Power Sources,* vol. 68, no. 1, pp. 91-98, Sep 1997, doi: 10.1016/s0378-7753(97)02575-5.

[39] H. J. S. Sand, "On the concentration at the electrodes in a solution, with special reference to the liberation of hydrogen by electrolysis of a mixture of copper sulphate and sulphuric acid," *The London, Edinburgh, and Dublin Philosophical Magazine and Journal of Science,* vol. 1, no. 1, pp. 45-79, 1901.

[40] G. Denuault, M. V. Mirkin, and A. J. Bard, "Direct determination of diffusion coefficients by chronoamperometry at microdisk electrodes," *Journal of electroanalytical chemistry and interfacial electrochemistry,* vol. 308, no. 1-2, pp. 27-38, 1991.

[41] M. W. Verbrugge and B. J. Koch, "Microelectrode investigation of ultrahigh-rate lithium deposition and stripping," *Journal of Electroanalytical Chemistry,* vol. 367, no. 1-2, pp. 123-129, 1994.

[42] D. Aurbach and Y. Cohen, "The application of atomic force microscopy for the study of Li deposition processes," (in English), *Journal of the Electrochemical Society,* Article vol. 143, no. 11, pp. 3525-3532, Nov 1996, doi: 10.1149/1.1837248.

[43] K. K. Fu *et al.*, "Toward garnet electrolyte-based Li metal batteries: An ultrathin, highly effective, artificial solid-state electrolyte/metallic Li interface," *Science Advances,* vol. 3, no. 4, Apr 2017, Art no. e1601659, doi: 10.1126/sciadv.1601659.

[44] A. Basile, A. I. Bhatt, and A. P. O'Mullane, "Stabilizing lithium metal using ionic liquids for long-lived batteries," *Nature Communications,* vol. 7, Jun 2016, Art no. 11794, doi: 10.1038/ncomms11794.

[45] Z. W. Seh, J. Sun, Y. M. Sun, and Y. Cui, "A Highly Reversible Room-Temperature Sodium Metal Anode," *Acs Central Science,* vol. 1, no. 8, pp. 449-455, Nov 2015, doi: 10.1021/acscentsci.5b00328.

[46] M. Kotobuki, H. Munakata, K. Kanamura, Y. Sato, and T. Yoshida, "Compatibility of Li7La3Zr2O12 Solid Electrolyte to All-Solid-State Battery Using Li Metal Anode," *Journal of the Electrochemical Society,* vol. 157, no. 10, pp. A1076-A1079, 2010, doi: 10.1149/1.3474232.

[47] S. Wenzel *et al.*, "Direct Observation of the Interfacial Instability of the Fast Ionic Conductor Li10GeP2S12 at the Lithium Metal Anode," *Chemistry of Materials,* vol. 28, no. 7, pp. 2400-2407, Apr 2016, doi: 10.1021/acs.chemmater.6b00610.

[48] D. Aurbach, "Review of selected electrode-solution interactions which determine the performance of Li and Li ion batteries," *Journal of Power Sources,* vol. 89, no. 2, pp. 206-218, Aug 2000, doi: 10.1016/s0378-7753(00)00431-6.

[49] R. Yazami, "Surface chemistry and lithium storage capability of the graphite-lithium electrode," *Electrochimica Acta,* vol. 45, no. 1-2, pp. 87-97, 1999, doi: 10.1016/s0013-4686(99)00195-4.

[50] X. Liu, J. Q. Huang, Q. Zhang, and L. Q. Mai, "Nanostructured Metal Oxides and Sulfides for Lithium-Sulfur Batteries," *Advanced Materials,* vol. 29, no. 20, May 2017, Art no. 1601759, doi: 10.1002/adma.201601759.

[51] H. J. Peng, J. Q. Huang, and Q. Zhang, "A review of flexible lithium-sulfur and analogous alkali metal-chalcogen rechargeable batteries," *Chemical Society Reviews,* vol. 46, no. 17, pp. 5237-5288, Sep 2017, doi: 10.1039/c7cs00139h.

[52] R. G. Cao, W. Xu, D. P. Lv, J. Xiao, and J. G. Zhang, "Anodes for Rechargeable Lithium-Sulfur Batteries," *Advanced Energy Materials,* vol. 5, no. 16, Aug 2015, Art no. 1402273, doi: 10.1002/aenm.201402273.

[53] X. Fang and H. S. Peng, "A Revolution in Electrodes: Recent Progress in Rechargeable Lithium-Sulfur Batteries," *Small,* vol. 11, no. 13, pp. 1488-1511, Apr 2015, doi: 10.1002/smll.201402354.

[54] M. Barghamadi *et al.*, "Lithium-sulfur batteries-the solution is in the electrolyte, but is the electrolyte a solution?," *Energy & Environmental Science,* vol. 7, no. 12, pp. 3902-3920, 2014, doi: 10.1039/c4ee02192d.

[55] W. Y. Li, G. Y. Zheng, Y. Yang, Z. W. Seh, N. Liu, and Y. Cui, "High-performance hollow sulfur nanostructured battery cathode through a scalable, room temperature, one-step, bottom-up approach," *Proceedings of the National Academy of Sciences of the United States of America,* vol. 110, no. 18, pp. 7148-7153, Apr 2013, doi: 10.1073/pnas.1220992110.

[56] H. H. Zheng, Q. N. Sun, G. Liu, X. Y. Song, and V. S. Battaglia, "Correlation between dissolution behavior and electrochemical cycling performance for LiNi1/3Co1/3Mn1/3O2-based cells," *Journal of Power Sources,* vol. 207, pp. 134-140, Jun 2012, doi: 10.1016/j.jpowsour.2012.01.122.

[57] G. Majeau-Bettez, T. R. Hawkins, and A. H. Stromman, "Life Cycle Environmental Assessment of Lithium-Ion and Nickel Metal Hydride Batteries for Plug-In Hybrid and Battery Electric Vehicles," *Environmental Science & Technology,* vol. 45, no. 10, pp. 4548-4554, May 2011, doi: 10.1021/es103607c.